Transportation Research Part C 183 (2026) 105432

Contents lists available at ScienceDirect

Transportation Research Part C

journal homepage: www.elsevier.com/locate/trc

Optimising toll prices based on a dynamic multi-region MFD SUE traffic model: formulation and a case study of Zealand, Denmark

Lawrence Christopher Duncan [a,*], Thomas Kjær Rasmussen [a], David Paul Watling [b], Ravi Seshadri [a]

[a] Department of Technology, Management and Economics, Technical University of Denmark, Akademivej Bygning 358, 2800 Kgs. Lyngby, Denmark
[b] Institute for Transport Studies, University of Leeds, 36-40 University Road, Leeds LS2 9JT, United Kingdom

ARTICLE INFO

Keywords:
Multi-region macroscopic fundamental diagram traffic model
Dynamic stochastic user equilibrium
Elastic demand
Departure time choice
Toll-price optimisation

ABSTRACT

Road use tolling is an effective way of alleviating congestion. Although many tolling models have been developed, there is gap in the research for a model that: i) is dynamic, ii) accounts for the impacts of tolls on travel demand and departure time choice, iii) accounts for stochasticity in travellers' route choices, iv) is well-behaved, producing continuous outputs, and v) is computationally feasible to apply to real-life large-scale networks. This paper fills this gap, by developing a tolling model based on the dynamic multi-region Macroscopic Fundamental Diagram (MFD) Stochastic User Equilibrium (SUE) traffic model introduced in Duncan et al. (2025). We begin by extending the model to account for elastic demand and departure time choice. Then, we integrate the model within a toll-price optimisation framework, where the tolling scheme is travel-time-based and the objective function maximises social welfare. We first test the model in a small-scale example multi-region MFD system, and then apply it to estimate an optimal toll-price in a real-life large-scale and detailed case study of Zealand, Denmark. Experiments find that the model is well-behaved and produces smooth objective function surfaces with a unique maximum. Travel behaviour implications of tolling are also realistic, where some travellers opt not to travel by car, some change their departure time, and some change their route. Results suggest that tolling could instigate a positive change in travel behaviour to benefit society.

1. Introduction

Traffic congestion is a recurring problem for societies. The many hours wasted in congestion each day results in huge economic losses, and has a negative impact on the environment and public health. An effective way of alleviating congestion is to encourage a change in travel behaviour through road use tolling (Liu et al., 2017; Zheng et al., 2016). Developing suitable models for evaluating tolling schemes is, however, a challenging task. To be behaviourally realistic, such a model should ideally: i) be dynamic, accounting for the propagation of traffic and time-dependent traffic conditions, ii) account for the impact of tolling on travel demand, iii) account for the impact of tolling on departure time choice, and iv) account for stochasticity in travellers' route choices. Many tolling models have been developed that exhibit some of these features, such as i) (Lu et al., 2008), ii) (Yang & Bell, 1997; Verhoef et al., 1996), iii) (Mahmassani & Herman, 1984; Arnott et al., 1990), iv) (Yang, 1999; Rambha & Boyles, 2016), ii) & iv) (Meng et al., 2012; Watling

* Corresponding author at: Department of Technology, Management and Economics, Technical University of Denmark, Akademivej Bygning 358, 2800 Kgs. Lyngby, Denmark.
E-mail address: lawdun@dtu.dk (L.C. Duncan).

https://doi.org/10.1016/j.trc.2025.105432
Received 28 February 2025; Received in revised form 24 October 2025; Accepted 29 October 2025
Available online 4 December 2025
0968-090X/© 2025 The Author(s). Published by Elsevier Ltd. This is an open access article under the CC BY license (http://creativecommons.org/licenses/by/4.0/).

et al., 2015), i) & iii) (Aboudina et al., 2016), i), ii) & iii) (Yang & Meng, 1998; Szeto & Lo, 2004), and a limited number exhibiting i), ii) iii), & iv) (Joksimovic et al., 2005; Lentzakis et al., 2020; Jing et al., 2024). For comprehensive reviews of tolling models, we direct the reader to de Palma & Lindsey (2011), Cheng et al. (2017), and Lombardi et al. (2021).

The issue, however, is that to be useable in real-life, the tolling model should ideally also be well-behaved, producing continuous outputs (e.g. route travel times / choice probabilities) as model inputs such as toll-price are varied, and computationally feasible to apply to real-life large-scale networks. Many detailed traffic models produce non-continuous outputs, especially outputs from traffic simulation software packages, which makes finding optimal toll-price solutions difficult. Moreover, many tolling models developed are only ever applied to small often synthetic networks (e.g. Yang & Meng, 2000; Yang, 1999; de Palma et al., 2005; Meng et al., 2012), and while it is not impossible to apply methodologies to large networks, and some have (e.g. Aboudina et al., 2016; Jing et al., 2024), adopting a detailed dynamic link-network-based approach makes efficient application unlikely. This limits the rigor in which analyses can be conducted. Jing et al. (2024), for example, explore different congestion pricing schemes on a large network using a large-scale microsimulator, but concede that computational intractability prevented them from optimising toll-prices.

In the current paper, we develop a tolling model that exhibits each of the four desirable behavioural features i)-iv) above, and is both well-behaved and computationally feasible, shown by successfully optimising toll-prices in a real-life large-scale case study. Rather than analysing tolling with a traditional 'microscopic' link-network traffic model, we use a more aggregate 'macroscopic' traffic modelling approach, where traffic conditions are captured over entire regions through Macroscopic Fundamental Diagrams (MFDs). The appeal of this approach is greater computational efficiency, easier calibration (Duncan et al, 2025), and suitability for analysing area-based tolling schemes, which most real-world tolling systems are (e.g. in Singapore, London, Stockholm, and Milan, see Gu et al., 2018 for an overview).

Region-based MFD traffic models have been used to model traffic in numerous traffic management studies, such as: route guidance management (Yildirimoglu et al., 2015; Knoop et al., 2012; Hosseinzadeh et al., 2023; Menelaou et al., 2023; Jiang et al., 2024; Chen et al., 2024), traffic control in urban networks (Geroliminis et al., 2012; Keyvan-Ekbatani et al., 2012,2015a,2015b; Ramezani et al., 2015; Haddad et al., 2013; Haddad, 2017a,2017b; Zhong et al., 2018a,b,2020; Guo & Ban, 2020; Batista et al., 2021; Fu et al., 2021; Yu et al., 2025; Sirmatel & Yildirimoglu, 2023; Sirmatel et al., 2021; Sirmatel & Geroliminis, 2021; Ren et al., 2020; He et al., 2024; Zhu et al., 2023; Kouvelas et al., 2023; Tsitsokas et al., 2023; de Souza et al., 2024; Jiang & Keyvan-Ekbatani, 2023; Keyvan-Ekbatani et al., 2021; Ding et al., 2025; Qian et al., 2024; Hamedmoghadam et al., 2022; Chen et al., 2024; Chen et al., 2022), parking management (Zheng and Geroliminis, 2016), vehicle dispatching (Ramezani & Nourinejad, 2018; Alisoltani et al., 2020,2021; Beojone & Geroliminis, 2021; Ramezani & Valadkhani, 2023; Valadkhani & Ramezani, 2023), tradable credit schemes (Balzer et al., 2023; Balzer and Leclercq, 2022), and emissions estimation (Barmpounakis et al., 2021; Batista & Leclercq 2020; Batista et al., 2022).

Although the research field on tolling with region-based MFD traffic models is growing, the literature is not vast. Geroliminis & Levinson (2009), Amirgholy & Gao (2017), and Daganzo & Lehe (2015) use a single-region MFD model to address the morning commute problem, using dynamic tolling to alter departure times to maximise outflow / user benefits. Lehe (2017) presents a static model of traffic into a single tolled downtown region with an MFD, in which commuters with varying trip lengths and benefits from driving decide between driving and a zero-utility outside option. Wang & Gayah (2021) use an MFD traffic model to explore cordon-tolling two urban regions to push traffic onto two motorway regions. Genser & Kouvelas (2022) use a multi-region MFD traffic model to identify optimal real-time dynamic tolls for maintaining system optimum. Zheng & Geroliminis (2013) use a multimodal-MFD model to optimise dedicated bus lane allocation and congestion pricing, and Zheng & Geroliminis (2020) adapt the work to maximise equity through different value of time groups. Parishad et al. (2025) employ reinforcement learning and a trip-based MFD model to develop a real-time dynamic cordon-based pricing scheme and evaluate its impact on travellers' mode choices.[1]

To the best of our knowledge, no study has developed a toll-price optimisation framework based on a dynamic multi-region MFD Stochastic User Equilibrium (SUE) traffic model accounting for elastic demand and departure time choice, and applied the model to optimise tolls in a real-life large-scale case study. The current paper fills this research gap. In Duncan et al. (2025) we developed a new dynamic multi-region MFD SUE traffic model and calibrated and applied it in a real-life large-scale and detailed case study of Zealand, Denmark with 135 regions and motorways considered separately. The current paper extends this model to account for both elastic demand and departure time choice, and then integrates it within a toll-price optimisation framework maximising social welfare. The tolling scheme explored is a 'time-based' scheme, meaning that the price paid depends on the travel time spent in the tolled area. The model and toll-price optimisation model are tested in an illustrative example and then applied to the real-life case study.

The paper is structured as follows. In Section 2 we introduce the dynamic multi-region MFD SUE traffic model developed in Duncan et al. (2025). In Section 3 we describe how a time-based toll can be captured by the model, as well as extend the model to account for elastic demand and departure time choice. In Section 4 we describe the solution method we use for solving the traffic equilibrium model. In Section 5 we integrate the model within a toll-price optimisation framework for maximising social welfare. In Section 6 we introduce the setup of the real-life case study, and in Section 7 we explore the optimal toll price in the case study and implications for travel behaviour. In Section 8 we discuss and provide thoughts on future research.

[1] The literature also includes numerous studies that use a traffic simulation software package (e.g. AIMSUM, MATSim) to simulate traffic given tolling in a single zone (Zheng et al., 2012, 2016; Simoni et al, 2014; Gu et al., 2018, 2019; Gu & Saberi, 2021; Chen et al., 2016, 2021; Dantsuji et al., 2019; Mansourianfar et al., 2021, 2024), multiple zones (Chen et al., 2024), or tolling expressway streets and arterial streets (Wei & Sun, 2018), and use an MFD to measure network performance. We do not class these though as using region-based MFD traffic models. They also require a traffic simulation package to be set up for the area and can come with considerable computational burden to run (Zheng et al, 2012; Gu & Saberi, 2021).

2. Dynamic multi-region MFD SUE model

In this section we give an overview of the dynamic multi-region MFD SUE model developed in Duncan et al. (2025), which we extend in Section 3 to model a tolling policy scheme and to account for tolling effects on elastic demand and departure time choice. For a more detailed description of the dynamic multi-region MFD SUE model we direct the reader to Sections 2-4 of Duncan et al. (2025).

The dynamic multi-region MFD SUE model has two components: a traffic propagation component and a traffic user equilibrium component, which feed back into each other. For a given setting of the route (regional path) flows, the traffic propagation component captures the journeys of vehicles from origin region to destination region over time and space, interacting with each other. This outputs experienced regional path travel times, which feed into the traffic user equilibrium component to determine regional path choice probabilities, outputting new regional path flows to feed back into the traffic propagation model.

A table of the nomenclature used in this paper can be found in Appendix A.

2.1. General multi-region MFD setup

An area of road network is partitioned into a set of regions R. The traffic conditions in each region $r \in R$ are described by a speed-MFD function $v_r(n_r)$, which describes the space-mean speed of vehicles in the region as a function of the total number of vehicles (accumulation), n_r, in the region at a given moment in time. As accumulation increases, average MFD speed decreases. Each region has an internal origin/destination, while regions with external borders may also have an external origin/destination (see Fig. 1). M is the set of regional Origin-Destination (OD) movements between each origin and destination. A regional path (otherwise termed r-path) is defined as a sequence of regions traversed when travelling an OD movement. P_m is the choice set of regional paths for OD movement $m \in M$. The total runtime period of the system (e.g. a morning, evening, or full day) is split into an indexed set Ψ of discrete time-slices, each with duration ε. The travel demands d_m^τ for each regional OD movement $m \in M$ departing during each time-slice $\tau \in \Psi$, are obtained by aggregating travel demands from the underlying network ODs over the time-slice between the OD regions. The travel demand d_m^τ for OD movement m departing during time-slice τ is split among the available regional paths $p \in P_m$ according to a regional path choice model, to give the regional path vehicle flows $f_{m,p}^\tau$. $\boldsymbol{f}$ is the vector of all r-path flows. Denote $l_{m,p,r}$ as the average distance travelled in region r (regional trip length) when travelling regional path $p \in P_m$, i.e. an average of the distances travelled by different link-routes on the underlying link-network through the region. For a given accumulation n_r in region r at a given entry time to the region, corresponding to an average MFD speed $v_r(n_r)$ in the region, the instantaneous travel time $t_{m,p,r}$ to cross region r when travelling r-path $p \in P_m$ is: $t_{m,p,r} = \frac{l_{m,p,r}}{v_r(n_r)}$.

2.2. Traffic propagation model

Embedded within the traffic user equilibrium model is a traffic propagation model based on utilising features of a Space-Time Graph (STG).[2] Here we shall briefly describe the model, for the full details we direct the reader to Section 3 of Duncan et al. (2025). Throughout each time-slice, demand is assumed to depart uniformly and continuously, and all drivers are assumed to experience the same speed in a region. Vehicles departing at the beginning and end of each time-slice travelling each regional path are tracked from origin to destination on the STG based on region travel times, see Fig. 2. Occupying STG areas of regional path flows are then used to calculate accumulation levels, which feed back to determine average vehicle speeds in a region during a time-slice (through the speed-MFD function), and thereby region travel times. The traffic propagation model is thus naturally expressed as a fixed-point problem in terms of region travel times.

Features/notation from the model that are relevant for the concepts in this paper are as follows:

- The constant time to cross region r when entering the region during time-slice τ travelling regional path $p \in P_m$ of OD movement m is denoted $t_{m,p,r}^\tau$. $\boldsymbol{t}$ is the vector of all region travel times.
- For a given regional path flow vector $\boldsymbol{f}$, $\boldsymbol{t}^*(\boldsymbol{f})$ is a region travel time vector solution to the traffic propagation fixed-point problem $\boldsymbol{t} = \boldsymbol{H}(\boldsymbol{t}, \boldsymbol{f})$ (see Eq. (4)) in Duncan et al. (2025)).
- For a given setting of the region travel times $\boldsymbol{t}$ and regional path flows $\boldsymbol{f}$, $\overline{n}_{m,p,r}^{\tau' \to \tau}(\boldsymbol{t}, \boldsymbol{f})$ is the average accumulation in region r during time-slice τ from the flow travelling regional path $p \in P_m$ departing during time-slice τ'.

[2] It is important to note that the model describes the traffic dynamics in a different way to the typical continuous-time inflow-outflow approach of which the accumulation (Daganzo, 2007; Geroliminis & Daganzo, 2008), trip (Arnott, 2013; Fosgerau, 2015; Lamotte & Geroliminis, 2016; Mariotte et al., 2017; Leclercq et al., 2017), and time-delay (Huang et al., 2020; Zhong et al., 2020) models are based. Although the traffic propagation model here is based on the same principle as the trip-based model, in that travellers' travel times depend on the time-varying traffic speeds over the course of the trip, the way in which we calculate the time-varying traffic speeds and model the traffic propagation are very different. The traffic propagation model here is a discrete-time model, designed to operate with coarse-grained time-slices (e.g. 15–60 min). The motivations for this are discussed in Section 1 of Duncan et al. (2025).

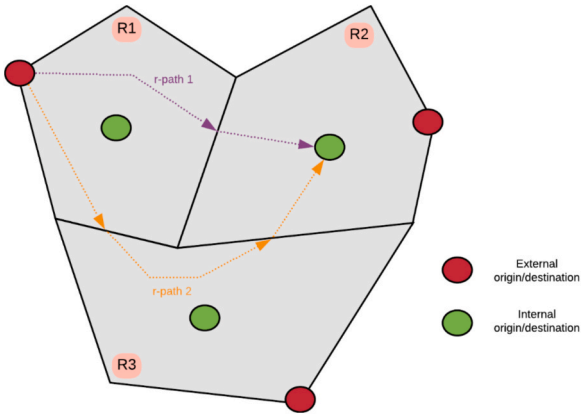

Fig. 1. Example area with a three-region partitioning, displaying two regional paths from the external origin of R1 to the internal destination of R2.

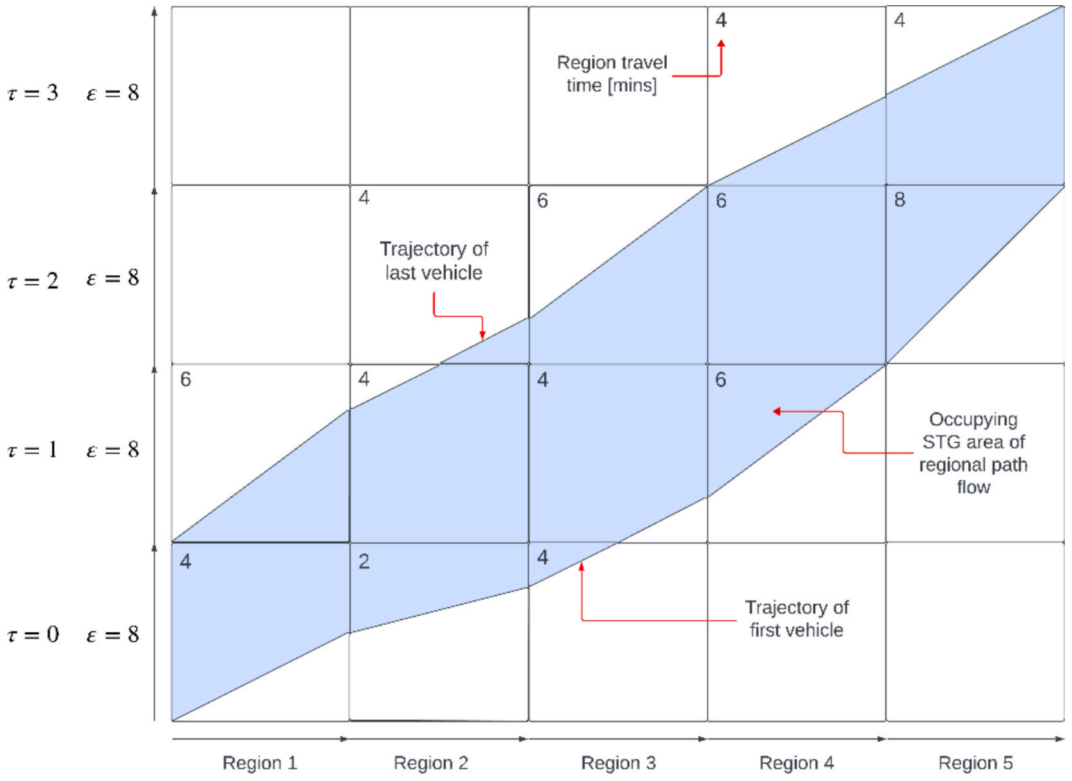

Fig. 2. Example of a flow trajectory on a space–time graph, for a regional path with 5 regions. Spatial X-axis is proportion of region completed and temporal Y-axis is proportion of time-slice completed (here each time-slice is $\varepsilon = 8$ mins).

- $\Psi^{\tau}_{m,p,r}$ is the set of active time-slices that some time is spent travelling in region r by any vehicle departing during time-slice τ travelling r-path $p \in P_m$ (e.g. in Fig. 2, region 4 is active during time-slices 1, 2, & 3: $\Psi^{0}_{1,1,4} = \{1, 2, 3\}$, and region 5 is active during time-slices 2 & 3: $\Psi^{0}_{1,1,5} = \{2, 3\}$).

As discussed in Section 3 of Duncan et al. (2025), the traffic propagation model satisfies desirable traffic flow theory properties such as First In, First Out (FIFO) and causality (partial causality within each time-slice and strict causality between time-slices). Note that in this study, congestion capacities and receiving capacities of regions are not considered, and thus there are no restrictions in the management of the outflow/inflow between adjacent regions.

Although the traffic propagation model is formulated as a fixed-point problem, in our solution method for solving the full dynamic multi-region MFD SUE model (described in Section 4), we do not fully solve the traffic propagation fixed-point problem for each new

setting of the regional path flows. It can be solved, however, by iteratively performing Steps 1–5 (the Traffic Propagation Stage) in Algorithm 1, and using either the Fixed-Point Iteration Method (Isaacson & Keller, 1966) or an averaging scheme to obtain the region travel times for the next iteration. In some experimentation we found the Fixed-Point Iteration Method worked well.

2.3. Traffic user equilibrium model

The Dynamic Multi-Region MFD SUE (D-MR-MFD-SUE) model embeds the traffic propagation model described in the previous section within an overall traffic user equilibrium model for equilibrating regional path traffic flows. Two versions of the model were derived in Duncan et al. (2025): in version 1 regional path choice is based on the region travel times at the current departing time-slice (i.e. instantaneous travel times), and in version 2 regional path choice is based on region travel times actually experienced at the time of travel (i.e. experienced travel times). Basing regional path choice on experienced travel times is more behaviourally realistic, as we supported empirically in Duncan et al. (2025). It is also more behaviourally realistic for elastic demand and departure time choice, corroborated in Remark 3.2 in Zhong et al. (2021). In this study we thus operate with experienced travel times.

One of the assumptions of the traffic propagation model is that the demand departs continuously and uniformly during the departing time-slice. As such, the demand experiences different travel times depending on when it departs during the time-slice. It is assumed though that the demand at each departing time-slice has the same regional path choice. Regional path choice is thus based upon the *average* experienced travel time from the flow departing at different times. The average experienced travel time of region r travelling r-path $p \in P_m$ departing during time-slice τ, $\bar{t}^{\tau}_{m,p,r}$, is calculated as follows:

$$\bar{t}^{\tau}_{m,p,r}(\boldsymbol{t},\boldsymbol{f}) = \sum\nolimits_{\tau' \in \Psi^{\tau}_{m,p,r}} \frac{\bar{n}^{\tau\to\tau'}_{m,p,r}(\boldsymbol{t},\boldsymbol{f})}{\sum_{\tau'' \in \Psi^{\tau}_{m,p,r}} \bar{n}^{\tau\to\tau''}_{m,p,r}(\boldsymbol{t},\boldsymbol{f})} \bullet t^{\tau'}_{m,p,r}, \tag{1}$$

where $\Psi^{\tau}_{m,p,r}$ is the set of active time-slices that some time is spent in traversing region r by any vehicle departing during time-slice τ travelling r-path $p \in P_m$. So, the average travel time of region r is a weighted average of the region travel times in succeeding time-slices the flow travels the region in, i.e. $t^{\tau'}_{m,p,r}$ for $\tau' \in \Psi^{\tau}_{m,p,r}$, where the weighting for succeeding time-slice τ' is its average contributing accumulation $\bar{n}^{\tau\to\tau'}_{m,p,r}$. See Section 4.3 of Duncan et al. (2025) for a demonstration. The total average experienced regional path travel time of r-path $p \in P_m$ when departing during time-slice τ is $\bar{T}^{\tau}_{m,p}(\boldsymbol{t},\boldsymbol{f}) = \sum_{r \in R_{m,p}} \bar{t}^{\tau}_{m,p,r}(\boldsymbol{t},\boldsymbol{f})$.

In general, the generalised region travel cost function is a weighted function of multiple travel cost attributes, including experienced travel time $\bar{t}^{\tau}_{m,p,r}(\boldsymbol{t},\boldsymbol{f})$. In this study, we specify the travel cost function for region r of r-path $p \in P_m$ when departing during time-slice τ as:

$$c^{\tau}_{m,p,r}(\boldsymbol{t},\boldsymbol{f}) = \alpha_{tt} \bullet \bar{t}^{\tau}_{m,p,r}(\boldsymbol{t},\boldsymbol{f}) + \alpha_{l} \bullet l_{m,p,r} \tag{2}$$

where $l_{m,p,r}$ is the regional trip length (in [km]) of region r travelling r-path $p \in P_m$, $\bar{t}^{\tau}_{m,p,r}$ is the average experienced travel time (in [min]) of region r when travelling r-path $p \in P_m$ departing at time-slice τ, α_{tt} is the Value of Time (VOT) (in [DKK/min]), and α_l is the Value of Distance (VOD) (in [DKK/km]). Therefore, $c^{\tau}_{m,p,r}$ is in units of [DKK]. The generalised travel cost of r-path $p \in P_m$ is $C^{\tau}_{m,p}(\boldsymbol{c}(\boldsymbol{t},\boldsymbol{f})) = \sum_{r \in R_{m,p}} c^{\tau}_{m,p,r}(\boldsymbol{t},\boldsymbol{f})$.

Regional path choice probabilities $Q^{\tau}_{m,p}$ are determined given the generalised region / regional path travel costs. In this study we adopt the same regional path choice model as adopted in Duncan et al. (2025), which is a modified version of the C-Logit model (Cascetta et al., 1996). For the formulation of the probability function and a discussion of its properties, as well as a discussion on what we believe regional path choice to represent, see Section 6.2.2 in Duncan et al. (2025).

D-MR-MFD-SUE conditions are formulated as follows:

D-MR-MFD-SUE: A r-path flow vector $\boldsymbol{f}^{*} \in F$ is a D-MR-MFD-SUE solution iff the flow departing during time-slice τ travelling r-path $p \in P_m$ of OD movement m, $f^{\tau,*}_{m,p}$, is a solution to the fixed-point problem

$$f^{\tau}_{m,p} = d^{\tau}_{m} \bullet Q^{\tau}_{m,p}(\boldsymbol{c}(\boldsymbol{t}^{*}(\boldsymbol{f}),\boldsymbol{f})), \quad \forall p \in P_m, \forall m \in M, \forall \tau \in \Psi, \tag{3}$$

where d^{τ}_{m} is the travel demand for OD movement m departing during τ, $Q^{\tau}_{m,p}$ is the choice probability function for r-path $p \in P_m$ and departing time-slice τ, and $c^{\tau}_{m,p,r}$ is as in (2), given $\boldsymbol{f}$ and $\boldsymbol{t}^{*}$ which is a region travel time solution to the traffic propagation fixed-point problem, given $\boldsymbol{f}$.

3. Tolling and travel demand extensions

3.1. Time-based tolling

Before extending the dynamic multi-region MFD SUE model to account for elastic demand and departure time choice, we first

introduce how tolling is captured within the model. Extending the cost function in (2) to include toll, the travel cost function for region r of r-path $p \in P_m$ when departing during time-slice τ is:

$$c^{\tau}_{m,p,r}(\boldsymbol{t},\boldsymbol{f}) = \alpha_{tt} \bullet \bar{t}^{\tau}_{m,p,r}(\boldsymbol{t},\boldsymbol{f}) + \alpha_{l} \bullet l_{m,p,r} + \kappa^{\tau}_{m,p,r}, \tag{4}$$

where $\kappa^{\tau}_{m,p,r}$ in [DKK] is the toll paid in region r by drivers departing during time-slice τ travelling r-path $p \in P_m$ of OD movement m.

In this study we consider a time-based toll. The reason for this is that this is the tolling scheme currently being explored in Denmark, the area of our case study. It is trivial to adapt the time-based toll to be distance-based (we shall describe how below), or cordon/area-based, and one can do this if one wishes.

For the time-based toll, a toll is imposed when travelling within certain regions of the multi-region MFD system, and the price of the toll depends on the time spent in the region. The policy could be implemented in several ways. Vehicles could be tracked in real-time, identifying when the vehicle enters and leaves a tolled region, and thus charging according to the time actually spent in the region and according to the toll-price at the time. This could be problematic though if there is for example an accident and drivers get charged an unfair amount. Drivers also like to know what they will pay before they set off. An alternative could therefore be to present drivers with a set of route options for the journey they are going to make giving them the toll cost for travelling each route, based on what the model predicts when departing at that time. The driver's journey is then tracked, and they are charged at the end based on the route they actually took and the time they departed, but using the model to predict the times they spent in the tolled regions and thus the toll they should pay.

Regardless of how the scheme is implemented, we must first model its implementation. Let ω^{τ}_{r} be the toll-price in [DKK/min] for travelling in region r during time-slice τ. $\boldsymbol{\omega}$ is the vector of all toll prices for all time-slices and regions. As described in Section 2.3, r-path flow experiences different region travel times depending on when it departs during the departing time-slice. Similarly, r-path flow experiences different tolls depending on when it departs during the departing time-slice. Depending on when the r-path flow departs (during the departing time-slice), a region may be traversed at different succeeding time-slices. As the travel times of the regions may be different at different succeeding time-slices, the travel times experienced may thus be different. And, as the toll-price may be different at different succeeding time-slices, the toll-price experienced may be different. We therefore calculate the average toll experienced by r-path flow departing during a time-slice. For a given region travel time vector $\boldsymbol{t}$ and r-path flow vector $\boldsymbol{f}$, the average time-based toll experienced in region r when departing during time-slice τ travelling regional path $p \in P_m$, $\kappa^{\tau}_{m,p,r}$, is calculated as follows:

$$\kappa^{\tau}_{m,p,r}(\boldsymbol{t},\boldsymbol{f},\boldsymbol{\omega}) = \sum\nolimits_{\tau' \in \Psi^{\tau}_{m,p,r}} \frac{\bar{n}^{\tau \to \tau'}_{m,p,r}(\boldsymbol{t},\boldsymbol{f})}{\sum_{\tau'' \in \Psi^{\tau}_{m,p,r}} \bar{n}^{\tau \to \tau''}_{m,p,r}(\boldsymbol{t},\boldsymbol{f})} \bullet t^{\tau'}_{m,p,r} \bullet \omega^{\tau'}_{r}. \tag{5}$$

So, the average toll experienced in region r is a weighted average of the tolls experienced in succeeding time-slices the flow travels the region in, i.e. $t^{\tau'}_{m,p,r} \bullet \omega^{\tau'}_{r}$ (time spent in region in [min] $\bullet$ toll price in [DKK/min]) for $\tau' \in \Psi^{\tau}_{m,p,r}$, where the weighting for succeeding time-slice τ' is its average contributing accumulation $\bar{n}^{\tau \to \tau'}_{m,p,r}$. As can be seen from (5), this is similar to how average experienced region travel times are calculated. The total average time-based toll experienced when travelling regional path $p \in P_m$ and departing during time-slice τ is: $K^{\tau}_{m,p}(\boldsymbol{t},\boldsymbol{f},\boldsymbol{\omega}) = \sum_{r \in R_{m,p}} \kappa^{\tau}_{m,p,r}(\boldsymbol{t},\boldsymbol{f},\boldsymbol{\omega})$. For a distance-based tolling scheme simply replace $t^{\tau'}_{m,p,r}$ in (5) with $l_{m,p,r}$.

With the time-based tolling scheme, $\kappa^{\tau}_{m,p,r}$ in the travel cost function in (4) is equal to $\kappa^{\tau}_{m,p,r}(\boldsymbol{t},\boldsymbol{f},\boldsymbol{\omega})$ in (5). Regional path travel costs thus depend on the tolling setting $\boldsymbol{\omega}$, and thus so do the regional path choice probabilities: $Q^{\tau}_{m,p} = Q^{\tau}_{m,p}(\boldsymbol{c}(\boldsymbol{t},\boldsymbol{f},\boldsymbol{\omega}))$. D-MR-MFD-SUE conditions with time-based tolling are as follows:

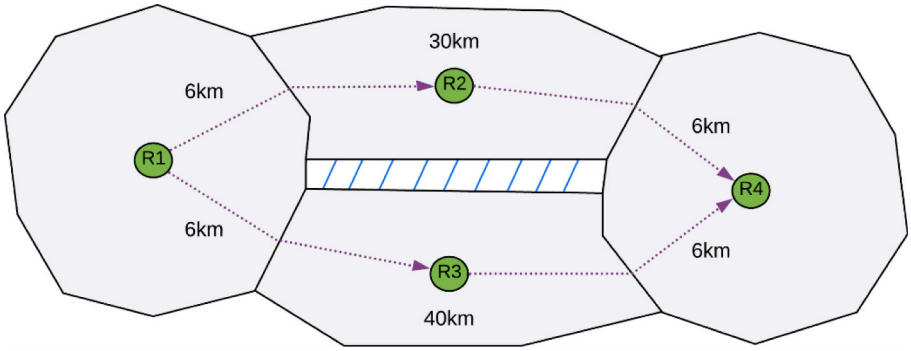

Fig. 3. Example multi-region MFD system.

D-MR-MFD-SUE: A r-path flow vector $\boldsymbol{f}^* \in F$ is a D-MR-MFD-SUE solution iff the flow departing during time-slice τ travelling r-path $p \in P_m$ of OD movement m, $f_{m,p}^{\tau,*}$, is a solution to the fixed-point problem

$$f_{m,p}^{\tau} = d_m^{\tau} \bullet Q_{m,p}^{\tau}(\boldsymbol{c}(\boldsymbol{t}^*(\boldsymbol{f}), \boldsymbol{f}, \boldsymbol{\omega})), \quad \forall p \in P_m, \forall m \in M, \forall \tau \in \Psi, \tag{6}$$

where d_m^{τ} is the travel demand for OD movement m departing during τ, and $Q_{m,p}^{\tau}$ is the choice probability function for r-path $p \in P_m$ and departing time-slice τ, and $c_{m,p,r}^{\tau}$ is as in (4), given $\boldsymbol{f}$, $\boldsymbol{\omega}$, and $\boldsymbol{t}^*$ which is a region travel time solution to the traffic propagation fixed-point problem.

To demonstrate how the model can capture the impacts of tolling on regional path choice, consider the small-scale example multi-region MFD system illustrated in Fig. 3. This small-scale example system will be used throughout the paper to demonstrate the different concepts we introduce, where we have set the system up to resemble the real-life case study in Section 6. There are 4 regions, 1 OD movement from region 1 to region 4, and two regional paths: RP1: $1 \rightarrow 2 \rightarrow 4$, RP2: $1 \rightarrow 3 \rightarrow 4$. For both r-paths, regions 1&4 have a regional trip length of 6 km, for r-path 1 region 2 has a regional trip length of 30 km, and for r-path 2 region 3 has a regional trip length of 40 km. The speed-MFD functions for each region assume the following functional form:

$$v_r(n_r) = (a-h)e^{-bn_r} + h,$$

where $a > 0$ gives the free-flow region speed, $b > 0$ determines the curve of the speed function, and h is the minimum speed. All regions have a free-flow speed of $a = 60$ km/hr and minimum speed of $h = 5$ km/hr. The curve parameters for regions 1–4 are $c = 0.001$, $c = 0.0005$, $c = 0.0003$, and $c = 0.001$, respectively. Fig. 4A plot the speed-MFD functions for regions 2&3, respectively. Throughout this paper, both in this example system and the real-life case study, the total runtime period is a day (1440 min) split into $\varepsilon = 30$ minute time-slices. Fig. 4B plots the demand profile over the course the day, where as can be seen there is a morning and evening peak. The values for VOT α_{tt} and VOD α_l are taken from the case study (see Section 8.2): $\alpha_{tt} = 1.99$[DKK/min] and $\alpha_l = 0.96$[DKK/km]. Unless specified otherwise, we also set the Logit scaling parameter θ and commonality scaling parameter ν for the C-Logit r-path choice model (see Section 6.2.2 in Duncan et al. (2025)) as those from the case study: $\theta = 0.0658$ and $\nu = 0.1389$.

We will compare the shift in travel behaviour predicted by the model from the No Tolling Scenario (NTS) (where there are no tolls) to a Tolling Scenario (TS) (where there is a toll enforced). Suppose that the toll imposed in the TS is upon travelling in region 2 during the morning/afternoon peaks between 7 and 9am and 3–6 pm (time-slices 14–17 and 30–35), with price 0.5 DKK/min. The toll-price vector $\boldsymbol{\omega}$ is thus set such that:

$$\omega_r^{\tau} = \begin{cases} 0.5 & \text{if } r \in \{2\} \text{ and } \tau \in \{x \in \mathbb{Z} : 14 \leq x \leq 17 \text{ or } 30 \leq x \leq 35\} \\ 0 & \text{otherwise} \end{cases}.$$

Fig. 5A displays the experienced travel times for regional paths 1&2 under the NTS and TS, when departing at different times across the day. Fig. 5B displays the regional path travel costs, and Fig. 5C displays the regional path choice probabilities. Under the NTS, regional path 1 is quicker than regional path 2 (see Fig. 5A), and therefore it has a cheaper travelling cost (see Fig. 5B) and most travellers choose it (see Fig. 5C). The travel time difference between the two regional paths is less during the peak hours due to congestion in region 2 of regional path 1, and therefore some flow switches to regional path 2. Under the TS, since the travel time of region 2 during the peak hours is around 40 mins, the time-based toll paid is around 20 DKK. This increases the travel cost of regional

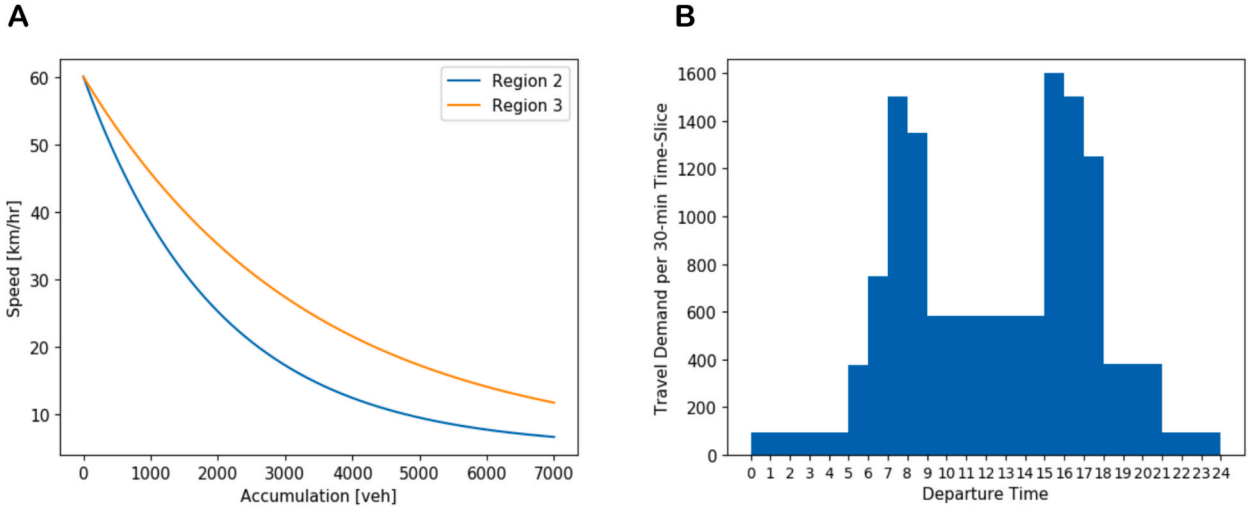

Fig. 4. A: Speed-MFD functions for regions 2 and 3. B: Travel demand departing at each 30-min time-slice over the course of the day.

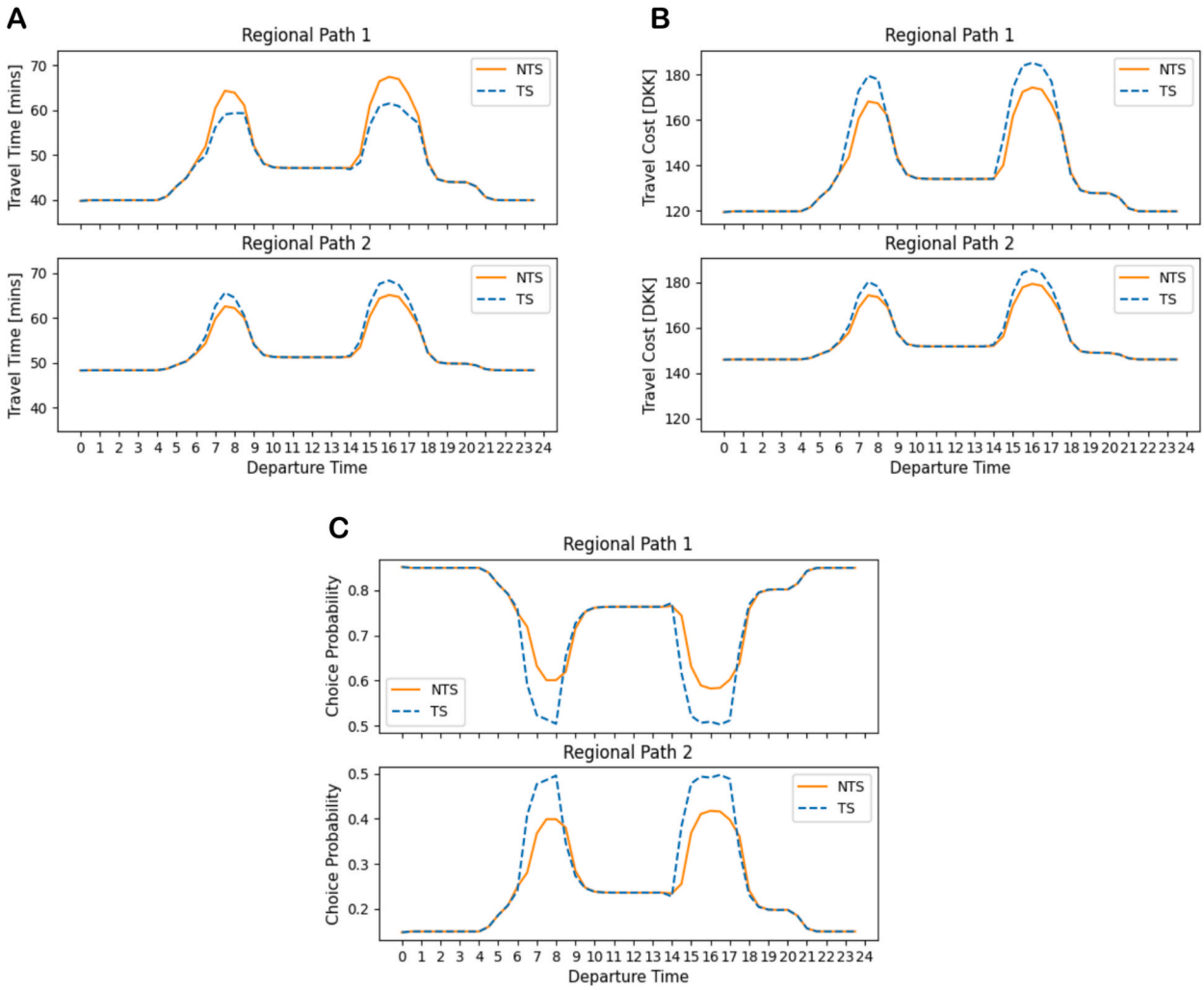

Fig. 5. Small-scale example system: Demonstrating the impact of tolling on regional path choice. A: Travel times of regional paths 1&2 under the NTS and TS, when departing at different times across the day. B: Regional path travel costs. C: Regional path choice probabilities.

path 1 when departing during and just before the peak hours (see Fig. 5B), pushing further travellers onto regional path 2 (see Fig. 5C), and thus decreasing the travel time of regional path 1 (see Fig. 5A).

3.2. Elastic demand

In this section we extend the dynamic multi-region MFD SUE model to account for elastic demand, i.e. to account for how travel demand may vary depending on the level of service (travelling costs). For example, increased costs for travelling a regional OD movement due to having to pay tolls may result in travellers opting to travel via a different mode of transport, or opting to cancel their trip, resulting in a decrease in the car travel demand. Contrastingly, decreased travelling costs due to improvements in regional path travel times from a reduction or displacement in traffic may attract travellers to travel by car, thus resulting in an increase in car travel demand.

To capture elastic demand, we adopt a traditional elastic demand function approach. The general approach is to compare the Level of Service (LoS) from the No Tolling Scenario (NTS) with that under tolling setting $\boldsymbol{\omega}$, and decrease/ increase the demand depending on how much the LoS worsens/improves. The LoS metric we use in this study is the expected travel cost for travelling the OD movement, obtained by weighting regional path travel cost by regional path choice probability.

Upon solution of the dynamic multi-region MFD SUE model in (6) where there are no tolls (the NTS), denote the equilibrated choice probability and travel cost of regional path $p \in P_m$ of OD movement m when departing during time-slice τ as $Q_{m,p}^{\tau,NTS}$ and $C_{m,p}^{\tau,NTS}$, respectively. Thus, under the NTS, the LoS (expected travel cost) of OD movement m when departing during time-slice τ is computed as follows:

$$\widetilde{C}_m^{\tau,NTS} = \sum\nolimits_{p\in P_m} Q_{m,p}^{\tau,NTS} \bullet C_{m,p}^{\tau,NTS}. \tag{7}$$

Now, with tolling, for a given setting of $\boldsymbol{t}, \boldsymbol{f}$, and $\boldsymbol{\omega}$, and thereby setting of the region travel costs $\boldsymbol{c}(\boldsymbol{t},\boldsymbol{f},\boldsymbol{\omega})$ from the travel cost function (4), the LoS (expected travel cost) of OD movement m when departing during time-slice τ is computed analogously as:

$$\widetilde{C}_m^{\tau}(\boldsymbol{c}(\boldsymbol{t},\boldsymbol{f},\boldsymbol{\omega})) = \sum\nolimits_{p\in P_m} Q_{m,p}^{\tau}(\boldsymbol{c}(\boldsymbol{t},\boldsymbol{f},\boldsymbol{\omega})) \bullet C_{m,p}^{\tau}(\boldsymbol{c}(\boldsymbol{t},\boldsymbol{f},\boldsymbol{\omega})). \tag{8}$$

The elastic demand function we assume is a power law function adopted in previous studies such as Watling et al. (2015) and Koh et al. (2013). This function was chosen as it gives constant elasticities. For a given setting of the regional path travel costs $\boldsymbol{c}(\boldsymbol{t},\boldsymbol{f},\boldsymbol{\omega})$, the elastic travel demand function for OD movement m and departing time-slice τ is:

$$\widetilde{d}_m^{\tau}(\boldsymbol{t},\boldsymbol{f},\boldsymbol{\omega}) = d_m^{\tau,NTS}\left(\frac{\widetilde{C}_m^{\tau}(\boldsymbol{c}(\boldsymbol{t},\boldsymbol{f},\boldsymbol{\omega}))}{\widetilde{C}_m^{\tau,NTS}}\right)^{-\gamma}, \tag{9}$$

where $\widetilde{C}_m^{\tau,NTS}$ and $\widetilde{C}_m^{\tau}$ are as in (7) and (8), respectively, $d_m^{\tau,NTS}$ is the travel demand for OD movement m departing at time-slice τ under the NTS, and $\gamma \geq 0$ is the demand elasticity parameter for car. The elastic demand function compares the level of service under the NTS $\widetilde{C}_m^{\tau,NTS}$ with the level of service under the tolling scenario $\widetilde{C}_m^{\tau}$ and increases or decreases the car demand depending on whether the level of service has improved or worsened with tolls. γ determines the rate at which demand is attracted to/away from car with an increase/decrease in the level of service (decrease/increase in expected minimum car travelling cost). Greater values of γ result in greater increases/decreases in demand for a given change in level of service.

D-MR-MFD-SUE conditions with toll-dependence and elastic demand are as follows:

D-MR-MFD-SUE: A r-path flow vector $\boldsymbol{f}^* \in F$ is a D-MR-MFD-SUE solution iff the flow departing during time-slice τ travelling r-path $p \in P_m$ of OD movement m, $f_{m,p}^{\tau,*}$, is a solution to the fixed-point problem

$$f_{m,p}^{\tau} = \widetilde{d}_m^{\tau}(\boldsymbol{c}(\boldsymbol{t}^*(\boldsymbol{f}),\boldsymbol{f},\boldsymbol{\omega}))) \bullet Q_{m,p}^{\tau}(\boldsymbol{c}(\boldsymbol{t}^*(\boldsymbol{f}),\boldsymbol{f},\boldsymbol{\omega}))), \quad \forall p \in P_m, \forall m \in \boldsymbol{M}, \forall \tau \in \Psi, \tag{10}$$

where $\widetilde{d}_m^{\tau}$ is the elastic travel demand function in (9) for OD movement m and departing time-slice τ and $Q_{m,p}^{\tau}$ is the choice probability function for r-path $p \in P_m$ and departing time-slice τ, given $\boldsymbol{f}$, $\boldsymbol{\omega}$, and $\boldsymbol{t}^*(\boldsymbol{f})$ which is a region travel time solution to the traffic propagation fixed-point problem, given $\boldsymbol{f}$.

To demonstrate how the elastic demand extension captures the impact of tolling on car travel demand, consider again the small-scale example multi-region MFD system in Fig. 3. Suppose again that the toll price is set as 0.5 DKK/min in region 2 between 7 and 9am and 3–6 pm. As shown in Fig. 5B, the travel costs are worse for both regional paths under the TS during the peak period. This means that the LoS will be worse when departing during the peak period, thus resulting in a decrease in car demand. Supposing that the demand elasticity parameter is $\gamma = 0.75$, Fig. 6A displays the percentage difference in travel demand across the day between the NTS and TS (where a negative number means there is less demand under the TS). As shown, the demand decreases for time-slices in which travellers travel in region 2 during the tolled peak hours. Demand increases slightly for time-slices around these decreased demand

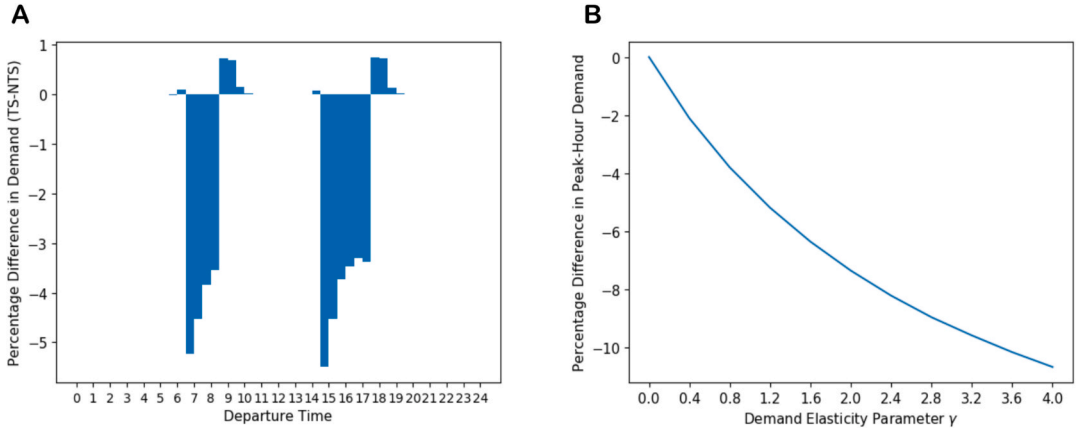

Fig. 6. Example system: demand changes under tolling from elastic demand. A: Percentage difference in demand between the NTS and TS at different times across the day (negative number implies less demand in the TS). B: Percentage difference in demand at 7–7:30am for different settings of the demand elasticity parameter γ.

time-slices. This is because, for example, less demand now departs between 8:30-9am as they will experience a toll, meaning accumulation levels are lower during 9–9:30am, meaning lower travel times/costs and thus a better level of service departing during 9–9:30am, resulting in induced demand.

Fig. 6B displays how the percentage difference in demand between the NTS and TS departing during 7:30-8am varies as the demand elasticity parameter γ is varied. As shown the peak-hour-departing demand decreases as γ is increased and travellers are more sensitive to increases in car travelling costs.

3.3. Departure time choice

With increased travelling costs from tolls, rather than opting to switch to other modes or cancel trip, car travel demand may instead choose to depart earlier or later to avoid tolling periods. We thus here extend the dynamic multi-region MFD SUE model further to account for departure time choice. The assumption we make is that the NTS is the 'ground truth', by which we mean that the dynamic multi-region MFD SUE solution with no tolls is assumed to be how people wish to behave, in terms of the travel demand and preferred departing/arrival times. We thus assume behaviour under the NTS is habitual and in a user equilibrium and so drivers know their travel costs when departing at their habitual departure time. Upon the introduction of tolls, we assume that travel behaviour will adjust to a new habitual user equilibrium, and given these new travel costs when departing at their preferred NTS departure time, travellers will either choose to mode switch / trip cancel or change their departure time. The assumption we make is that travellers first choose whether they will mode switch / cancel trip, and then, if continuing to travel by car, choose whether to adjust their departure time. As such, the demands and travelling costs from the departure time choice model feed into the elastic demand function, rather than elastic demand feeding into the departure time choice. Fig. 7 illustrates the assumed decision-making process of travellers.

We shall begin by defining the departure time utility function, which is inspired by such functions in Cantelmo & Viti (2019), Dantsuji et al. (2021). The OD movement m utility of departing during time-slice τ given the driver departs during time-slice τ' under the NTS is as follows:

$$Y_m^{\tau' \to \tau}(\boldsymbol{t}, \boldsymbol{f}, \boldsymbol{\omega}) = -\overline{T}_m^{\tau}(\boldsymbol{t}, \boldsymbol{f}) - \frac{\alpha_{early}^{\tau}}{\alpha_{tt}}\left(PAT_m^{\tau', NTS} - AT_m^{\tau}(\boldsymbol{t}, \boldsymbol{f})\right)_+ - \frac{\alpha_{late}^{\tau}}{\alpha_{tt}}\left(AT_m^{\tau}(\boldsymbol{t}, \boldsymbol{f}) - PAT_m^{\tau', NTS}\right)_+ - \frac{1}{\alpha_{tt}}K_m^{\tau}(\boldsymbol{t}, \boldsymbol{f}, \boldsymbol{\omega}). \tag{11}$$

$PAT_m^{\tau', NTS}$ is the OD movement m aggregate Preferred Arrival Time (PAT) when departing during time-slice τ' in the NTS, and, under toll setting $\boldsymbol{\omega}$:

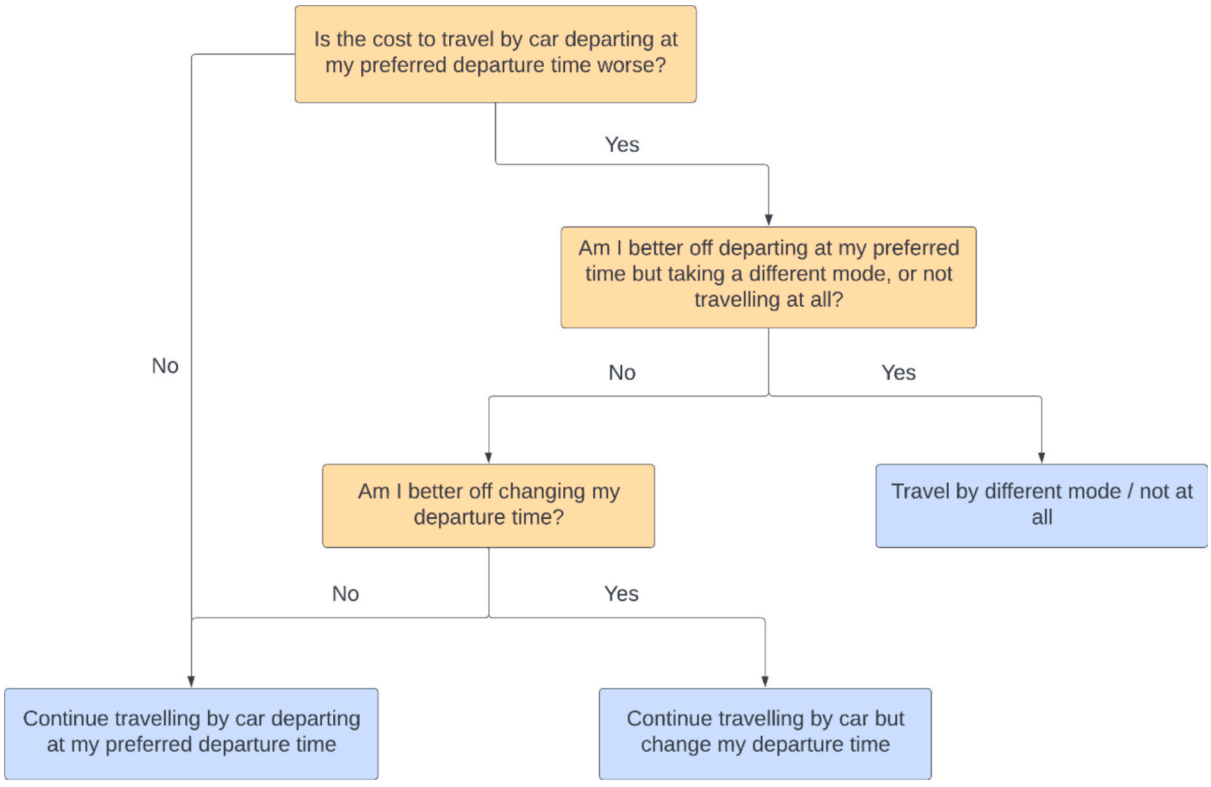

Fig. 7. Assumed decision-making process of travellers.

- $\overline{T}_m^\tau$ is the average experienced travel time of OD movement m when departing during time-slice τ,
- AT_m^τ is the aggregate Arrival Time (AT) of OD movement m when departing during time-slice τ,
- K_m^τ is the average toll experienced when departing during time-slice τ travelling OD movement m.

α_{tt} is VOT in [DKK/min] (the same as in (4)), α_{early}^τ is the value of arriving early in [DKK/min] when departing during time-slice τ in the NTS, and α_{late}^τ is the value of arriving late in [DKK/min] when departing during time-slice τ in the NTS. $\frac{\alpha_{early}^\tau}{\alpha_{tt}}$ and $\frac{\alpha_{late}^\tau}{\alpha_{tt}}$ are therefore the relative values of arriving early and late, respectively, compared to VOT. These give the ratio of the value of being early/late by 1 min to the value of 1 min of travel time. In the small-scale system and real-life case study in the current paper we consider a full work-day time horizon where there is a morning and afternoon commute. We assume that in the morning there is a greater penalty for arriving late, and in the afternoon there is a greater penalty for arriving early (leaving early). The values we adopt throughout the paper were taken from Small (1982), and adopted in numerous other studies such as Dantsuji et al. (2021). For time-slices τ before midday, $\frac{\alpha_{early}^\tau}{\alpha_{tt}} = 0.609$ and $\frac{\alpha_{late}^\tau}{\alpha_{tt}} = 2.377$, while for time-slices τ after midday, $\frac{\alpha_{early}^\tau}{\alpha_{tt}} = 2.377$ and $\frac{\alpha_{late}^\tau}{\alpha_{tt}} = 0.609$. Note that since K_m^τ is in units of [DKK] (see below), $Y_m^{\tau' \to \tau}$ is in units of time [min].

Since we assume that the NTS is the ground truth, PATs are obtained from r-path travel times from the dynamic multi-region MFD SUE solution with no tolls. Denote the experienced travel time of r-path $p \in P_m$ when departing during time-slice τ' under the NTS as $\overline{T}_{m,p}^{\tau',NTS}$, obtained from the equilibrated region travel times $\boldsymbol{t}^*$ and r-path flows $\boldsymbol{f}^*$ upon solution of (6) with $\boldsymbol{\omega} = 0$ (see Section 3). The average travel time of OD movement m when departing during time-slice τ' under the NTS is calculated by averaging the r-path travel times for that OD movement:

$$\overline{T}_m^{\tau',NTS} = \sum\nolimits_{p \in P_m} Q_{m,p}^{\tau',NTS} \bullet \overline{T}_{m,p}^{\tau',NTS}, \tag{12}$$

where $Q_{m,p}^{\tau',NTS}$ is the choice probability of r-path $p \in P_m$ when departing during τ' under the NTS. The average OD movement travel time is therefore a weighted average of the r-path travel times, weighted by r-path choice probability. For a demand departing during time-slice τ', it is assumed for simplicity that the departure time is at the half-way point of the time-slice, so that a single PAT can be obtained. Thus, if t_0 is the initial real time of the runtime period and ε is the time-slice duration, then the assumed departure time of a demand departing during time-slice τ' is $(t_0 + \tau' \bullet \varepsilon + t_0 + (\tau' + 1) \bullet \varepsilon)/2$, where $t_0 + \tau' \bullet \varepsilon$ and $t_0 + (\tau' + 1) \bullet \varepsilon$ are the beginning and end times of the time-slice, respectively. Therefore, the aggregate PAT of the demand travelling OD movement m and departing during time-slice τ' under the NTS is:

$$PAT_m^{\tau'} = \frac{t_0 + \tau' \bullet \varepsilon + t_0 + (\tau' + 1) \bullet \varepsilon}{2} + \overline{T}_m^{\tau',NTS}. \tag{13}$$

While the PATs are exogenous, fixed as inputs into the system, $\overline{T}_m^\tau$, AT_m^τ, and K_m^τ in (11) are endogenous, dependent upon $\boldsymbol{t}, \boldsymbol{f}$, and $\boldsymbol{\omega}$.

$\overline{T}_m^\tau$ is calculated by averaging the experienced r-path travel times (see Section 2.3) for that OD movement:

$$\overline{T}_m^\tau(\boldsymbol{t}, \boldsymbol{f}, \boldsymbol{\omega}) = \sum\nolimits_{p \in P_m} Q_{m,p}^\tau(\boldsymbol{c}(\boldsymbol{t}, \boldsymbol{f}, \boldsymbol{\omega}))) \bullet \overline{T}_{m,p}^\tau(\boldsymbol{t}, \boldsymbol{f}), \tag{14}$$

where $Q_{m,p}^\tau(\boldsymbol{c}(\boldsymbol{t}, \boldsymbol{f}, \boldsymbol{\omega}))$ is the choice probability of r-path $p \in P_m$ when departing during τ.

K_m^τ is calculated in a similar fashion:

$$\mathrm{K}_m^\tau(\boldsymbol{t}, \boldsymbol{f}, \boldsymbol{\omega}) = \sum\nolimits_{p \in P_m} Q_{m,p}^\tau(\boldsymbol{c}(\boldsymbol{t}, \boldsymbol{f}, \boldsymbol{\omega}))) \bullet \mathrm{K}_{m,p}^\tau(\boldsymbol{t}, \boldsymbol{f}, \boldsymbol{\omega}), \tag{15}$$

where $\mathrm{K}_{m,p}^\tau$ is the total average toll experienced when travelling regional path $p \in P_m$ and departing during time-slice τ (see Section 3).

Given the average OD movement travel time $\overline{T}_m^\tau$, the aggregate AT of the demand travelling OD movement m and departing during time-slice τ is:

$$AT_m^\tau(\boldsymbol{t}, \boldsymbol{f}) = \frac{t_0 + \tau \bullet \varepsilon + t_0 + (\tau + 1) \bullet \varepsilon}{2} + \overline{T}_m^\tau(\boldsymbol{t}, \boldsymbol{f}). \tag{16}$$

$\left(PAT_m^{\tau',NTS} - AT_m^\tau(\boldsymbol{t}, \boldsymbol{f})\right)_+$ and $\left(AT_m^\tau(\boldsymbol{t}, \boldsymbol{f}) - PAT_m^{\tau',NTS}\right)_+$ in (11) are therefore the aggregate amount of time an OD movement m traveller will arrive early and arrive late, respectively, when departing during time-slice τ given they depart during time-slice τ' in the NTS.

Now, for the departure time choice, we assume a Multinomial Logit (MNL) choice model, chosen because of its simple closed-form probability function. MNL may potentially miss correlations between departure time alternatives, though we consider large time-slices in our dynamic traffic model where correlation is likely to be less. Moreover, in an empirical study, Steed & Bhat (2000) found that an Ordered Generalised Extreme Value correlation-based model gave unrealistic estimates, and that, for all trip-type categories, MNL was

adequate in representing departure time choice in terms of data fit. Several other studies have also found MNL to be reasonable (de Palma et al., 1983; Small, 1982; Abkowitz, 1980). Thus, supposing that travellers choose from all time-slices throughout the day, for given a set of departure time utilities $\boldsymbol{Y}$, the probability that an OD movement m traveller chooses to depart during time-slice τ, given that they depart during time-slice τ' under the NTS, is as follows:

$$\pi_m^{\tau' \to \tau}(\boldsymbol{Y}(\boldsymbol{t},\boldsymbol{f},\boldsymbol{\omega})) = \frac{\exp\left(\mu Y_m^{\tau' \to \tau}(\boldsymbol{t},\boldsymbol{f},\boldsymbol{\omega})\right)}{\sum_{\tau'' \in \Psi} \exp\left(\mu Y_m^{\tau'' \to \tau}(\boldsymbol{t},\boldsymbol{f},\boldsymbol{\omega})\right)}, \tag{17}$$

where Ψ is the set of time-slices, $Y_m^{\tau' \to \tau}$ is the OD movement m utility of departing during time-slice τ given the driver departs during time-slice τ' under the NTS, and $\mu > 0$ is a departure time choice Logit scaling parameter.

Given our assumption that travellers first choose whether they will mode switch / trip cancel, and then if continuing to travel by car whether to change their departure time, the demand travelling OD movement m choosing to depart during time-slice τ is calculated as follows:

$$\widetilde{d}_m^{\tau,DTC}(\boldsymbol{t},\boldsymbol{f},\boldsymbol{\omega}) = \sum\nolimits_{\tau' \in \Psi} \pi_m^{\tau' \to \tau}(\boldsymbol{Y}(\boldsymbol{t},\boldsymbol{f},\boldsymbol{\omega})) \bullet \widetilde{d}_m^{\tau'}(\boldsymbol{c}(\boldsymbol{t},\boldsymbol{f},\boldsymbol{\omega})), \tag{18}$$

where $\pi_m^{\tau' \to \tau}$ is as in (17) and $\widetilde{d}_m^{\tau'}$ is as in (9). The total demand departing during time-slice τ is thus obtained by summing up the demands that, having chosen to continue travelling by car, choose to depart at that time-slice. Note that the average NTS OD movement travelling costs $\widetilde{C}_m^{\tau,NTS}$ in $\widetilde{d}_m^{\tau'}$ in (9) for departure time choice are those from solving dynamic multi-region MFD SUE with departure time choice, but without elastic demand (i.e. (19) below with $\gamma = 0$).

D-MR-MFD-SUE conditions with toll-dependence, elastic demand, and departure time choice are as follows:

D-MR-MFD-SUE: A r-path flow vector $\boldsymbol{f}^* \in F$ is a D-MR-MFD-SUE solution iff the flow departing during time-slice τ travelling r-path $p \in P_m$ of OD movement m, $f_{m,p}^{\tau,*}$, is a solution to the fixed-point problem

$$f_{m,p}^{\tau} = \widetilde{d}_m^{\tau,DTC}(\boldsymbol{t}^*(\boldsymbol{f}),\boldsymbol{f},\boldsymbol{\omega}) \bullet Q_{m,p}^{\tau}(\boldsymbol{c}(\boldsymbol{t}^*(\boldsymbol{f}),\boldsymbol{f},\boldsymbol{\omega})), \quad \forall p \in P_m, \forall m \in M, \forall \tau \in \Psi, \tag{19}$$

where $\widetilde{d}_m^{\tau,DTC}$ is the departure time choice travel demand function in (18) for OD movement m and departing time-slice τ and $Q_{m,p}^{\tau}$ is the choice probability function for r-path $p \in P_m$ and departing time-slice τ, given $\boldsymbol{f}$, $\boldsymbol{\omega}$, and $\boldsymbol{t}^*(\boldsymbol{f})$, which is a region travel time solution to the traffic propagation fixed-point problem, given $\boldsymbol{f}$.

To demonstrate how the departure time choice extension captures the impact of tolling on departure time choice, consider again the small-scale example multi-region MFD system in Fig. 3. Suppose again that the toll price is set as 0.5 DKK/min in region 2 between 7 and 9am and 3–6 pm. Suppose the demand elasticity parameter is $\gamma = 0.7$ and departure time choice Logit scaling parameter is $\mu = 3$. Fig. 8A displays, given the departure time choice, the travel demand under the NTS departing at each 30-min time-slice across the day. As shown, the demand profile resembles the original demand profile in Fig. 4B, but with some demand during the peaks shifted to

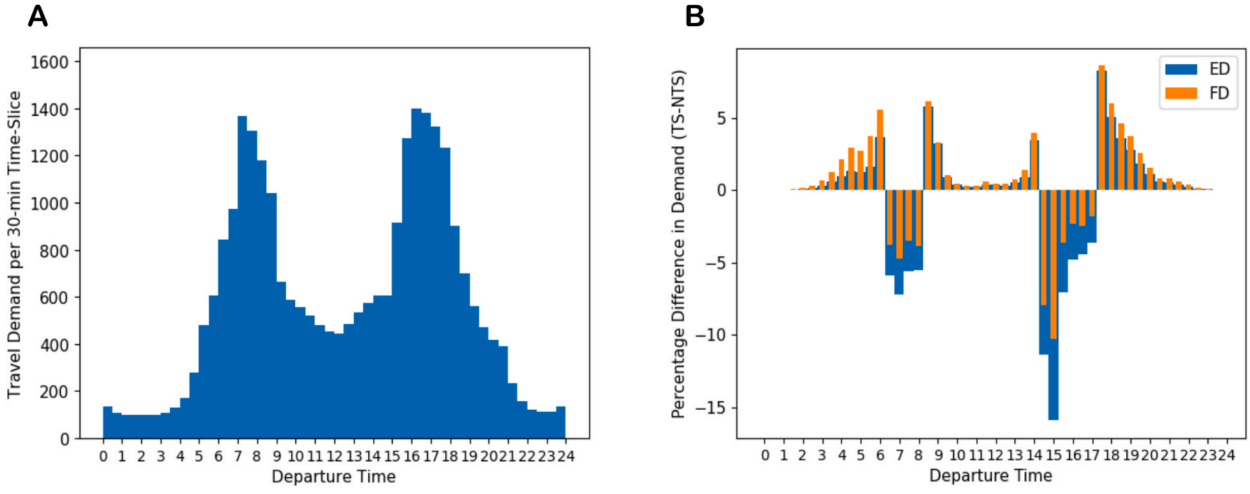

Fig. 8. Small-scale example system: Departure time choice demands. A: Travel demand per 30-min time-slice departing across the day with departure time choice under the NTS. B: Percentage difference in demand between the NTS and TS at different times across the day, with fixed demand and with elastic demand (negative number implies less demand in TS).

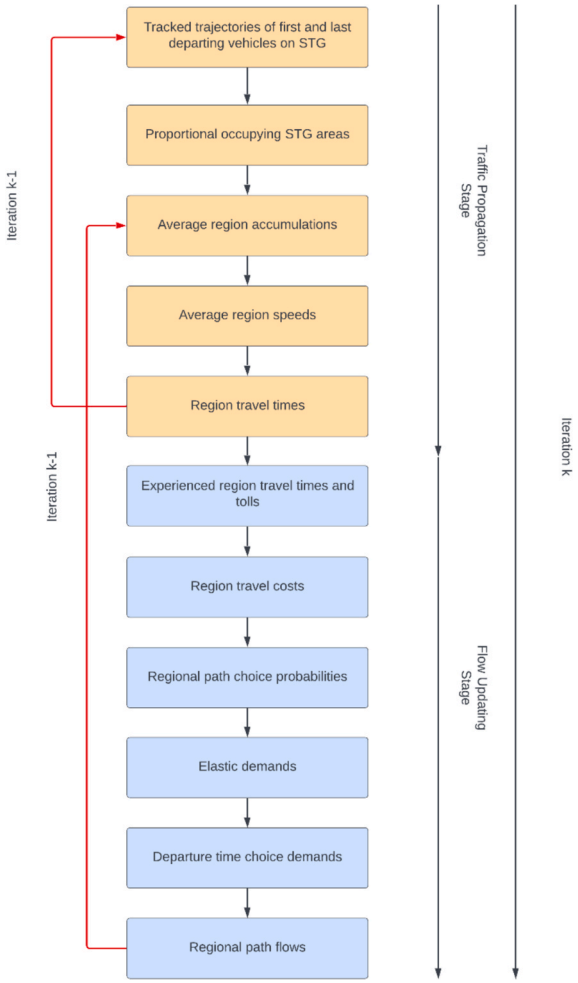

Fig. 9. Schematic diagram illustrating overall solution method for solving D-MR-MFD-SUE with elastic demand and departure time choice.

earlier/later. Fig. 8B displays the percentage difference in travel demand across the day between the NTS and TS, with fixed demand (FD) and with elastic demand (ED). As shown, for the morning and afternoon commutes, some demand departs earlier or later to avoid the tolling period. More demand departs earlier in the morning and later in the evening due to the greater arriving late / leaving early penalties. With elastic demand, the demand departing during the peaks is even less in the TS.

4. Traffic equilibrium solution methodology

4.1. Solution method

Here we introduce the method we adopt for solving the traffic equilibrium model, for a given setting of the tolls. This is not to be confused with the solution method for solving the toll optimisation problem, which will be discussed in Section 5.3.

In Duncan et al. (2025) a solution method was proposed for solving the standard D-MR-MFD-SUE model without elastic demand and departure time choice (see Section 4.4 of that paper). Here, we extend the method to solve D-MR-MFD-SUE with elastic demand and departure time choice by adding additional steps. Pseudo-code for the solution method is given in Algorithm 1, and Fig. 9 presents a schematic diagram illustrating the method. As evident from (19), the D-MR-MFD-SUE model is a fixed-point problem embedded within another fixed-point problem. This gives rise in our algorithm to an inner-loop involving region travel times $\boldsymbol{t}$, and an outer-loop involving the r-path flows $\boldsymbol{f}$. As shown in Algorithm 1 and Fig. 9, there is thus a Traffic Propagation Stage to update the region travel times given the current r-path flows, and then a Flow Updating Stage to update r-path flows given the updated region travel times from the traffic propagation model.

One solution method could be to fully solve at every outer iteration the inner traffic propagation fixed-point problem in (19) for each set of updated r-path flows. For example, in the schematic diagram in Fig. 9, at master iteration k one could perform a series of inner-loops between tracking trajectories of first departing vehicles and computing region travel times, for fixed r-path flows.

However, tracking vehicle trajectories is the most computation time consuming part, and thus in the method we propose we try to minimise this. As illustrated in Fig. 9, we instead propose that, at each master iteration k, just one loop / run-through of the traffic propagation steps is performed updating the region travel times, which feed into updating the r-path flows.

For details on the flow-averaging scheme and convergence criteria we utilise in this study, see Section 4.4 of Duncan et al. (2025).

Algorithm 1. Pseudo-code for solving D-MR-MFD-SUE with elastic demand and departure time choice

Step 0: *Initialisation*. Initialise the r-path region travel time vector $\boldsymbol{t}^{(0)}$ and r-path flow vector $\boldsymbol{f}^{(0)}$ for iteration $k = 0$. Set $k = 1$.
For iteration k:

Traffic Propagation Stage

Step 1: *Track trajectories of first departing vehicles*. Given the r-path region travel time vector $\boldsymbol{t}^{(k-1)}$ from iteration $k-1$, for each r-path for each OD movement, track the trajectories of the first vehicle departing at the beginning of each time-slice $\tau \in \Psi$, plus the trajectory of the last vehicle departing at the end of the last departing time-slice in Ψ (see Appendix C.1 in Duncan et al. (2025)).

Step 2: *Compute proportional occupying STG areas*. Given the tracked vehicle trajectories in the previous step, calculate the proportional occupying STG areas (see Appendix C.2 in Duncan et al. (2025)).

Step 3: *Compute average region accumulations*. Given the r-path region travel time vector $\boldsymbol{t}^{(k-1)}$ and r-path flow vector $\boldsymbol{f}^{(k-1)}$ from iteration $k-1$, and the proportional occupying STG areas computed in the previous step, compute the average contributing accumulations from each r-path flow, and thereby the total average region accumulations (see Eqs. (3) and (2) in Duncan et al. (2025)).

Step 4: *Compute average region speeds*. Given the average region accumulations computed in the previous step, compute the average region speeds (see Eq. (1)) in Duncan et al. (2025)).

Step 5: *Update region travel times*. Given the average region speeds computed in the previous step, update the r-path region travel time vector $\boldsymbol{t}^{(k)}$ for iteration k (see Eq. (4)) in Duncan et al. (2025)).

Flow Updating Stage

Step 6: *Compute experienced region travel times and tolls*. Given the updated r-path region travel times $\boldsymbol{t}^{(k)}$ for iteration k, and the average region accumulations computed in Step 3, compute the experienced region travel times (see Eq. (1)) and experienced region tolls (see Eq. (5)).

Step 7: *Compute region travel costs*. Given the experienced region travel times and tolls computed in the previous step, compute the region travel costs (see Eq. (4)).

Step 8: *Compute r-path choice probabilities*. Given the region travel costs computed in the previous step, compute the r-path choice probabilities (see e.g. Eq. (13)) in Duncan et al. (2025)).

Step 9: *Compute elastic demands*.

Step 9.1: Given the r-path choice probabilities computed in the previous step and the region travel costs computed in Step 7, compute the average OD movement travel costs (see Eq. (8)).

Step 9.2: Given these, compute the elastic demands (see Eq. (9)).

Step 10: *Compute departure time choice demands*.

Step 10.1: Given the experienced region travel times and tolls computed in Step 6, compute average OD movement ATs (see Eq. (16)) and tolls experienced (see Eq. (15)).

Step 10.2: Given these and the NTS PATs, compute the departure time utilities (see Eq. (11)).

Step 10.3: Given these, compute the departure time choice probabilities (see Eq. (17)).

Step 10.4: Given these and the elastic demands computed in Step 9, compute the departure time choice demands (see Eq. (18))

Step 11: *Update r-path flows*. Given the r-path choice probabilities computed in Step 8 and the travel demands computed in Steps 9–10, compute auxiliary r-path flows and perform some averaging scheme to update the r-path flow vector $\boldsymbol{f}^{(k)}$ for iteration k.

Step 12: *Check for convergence*. If convergence criteria are met for $\boldsymbol{t}^{(k)}$ and $\boldsymbol{f}^{(k)}$ (see e.g. Eqs. (8) and (9) in Duncan et al. (2025)), stop. Otherwise, set $k = k+1$ and continue to next iteration.

4.2. Convergence demonstration

Here we shall provide empirical support that Algorithm 1 converges to a D-MR-MFD-SUE solution. Fig. 10A–B demonstrate for the

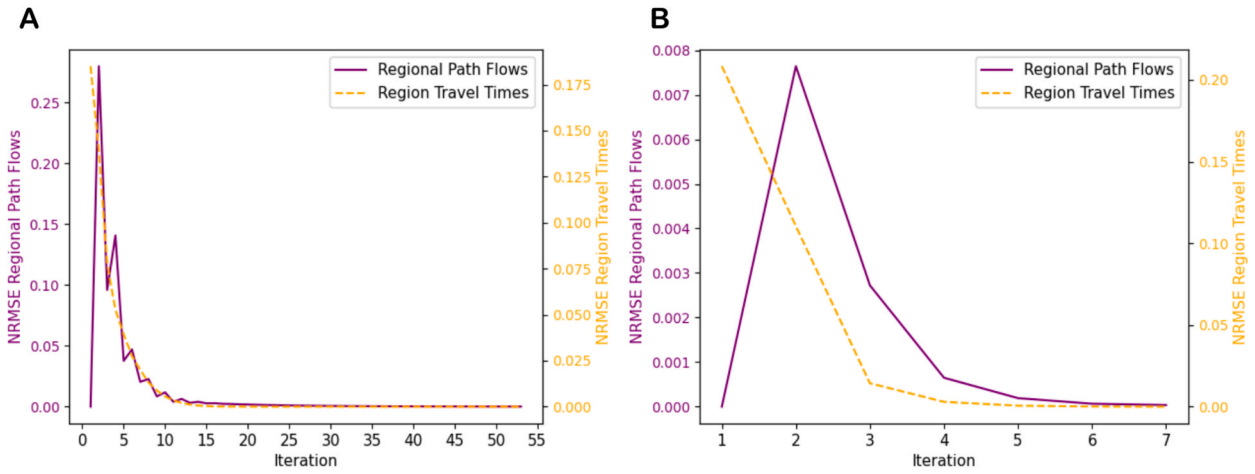

Fig. 10. Demonstrating convergence of Algorithm 1 for solving D-MR-MFD-SUE with elastic demand and departure time choice. A: Example system. B: Real-life case study.

small-scale example system in Fig. 3 and real-life case study (see Sections 6 & 7), respectively, convergence of Algorithm 1 solving D-MR-MFD-SUE with elastic demand and departure time choice. For the small-scale example system the model/toll specifications are the same as those for Fig. 8C, and for the real-life case study the model specifications are as discussed in Section 6.2, with the toll-price set as the optimised value of 4.544 DKK/min (see Section 7). Fig. 10 displays the regional path flow and region travel time Normalised Root Mean Squared Error (NMRSE) convergence measures (see Section 4.4 in Duncan et al. (2025)) at each iteration of Algorithm 1. As can be seen, both measures converge to zero, demonstrating successful convergence.

5. Social welfare optimisation framework

5.1. Objective function

The objective function we consider in this study is a classical social welfare function, that has been used in a variety of studies such as Huang et al. (2000), Ying & Yang (2005), Meng et al. (2012), and Watling et al. (2015), where detailed discussions of the derivation of this measure can be found. The objective function to maximise is as follows:

$$Z_{SW}(\boldsymbol{\omega}) = \underbrace{Z_{ID}(\boldsymbol{t},\boldsymbol{f},\boldsymbol{\omega}) + Z_{LoS}(\boldsymbol{t},\boldsymbol{f},\boldsymbol{\omega})}_{Consumer} + \underbrace{Z_{TR}(\boldsymbol{t},\boldsymbol{f},\boldsymbol{\omega})}_{Producer}, \tag{20}$$

where Z_{ID} is the Inverse Demand component of consumer surplus, Z_{LoS} is the LoS component of consumer surplus, and Z_{TR} is the Toll Revenue component representing the producer surplus. These will be specified in turn below, noting that we specify the objective function as relative to a base case, which is social welfare under the NTS. The interpretation of the objective function is therefore the gain in social welfare from the NTS.

The Inverse Demand component of Z_{SW} captures the disbenefit from not travelling by car due to tolling. Without departure time choice, given the power law elastic demand function assumed in (9), the inverse demand function for OD movement m time-slice τ is as follows for a demand x:

$$g_m^\tau(x) = \widetilde{C}_m^{\tau,NTS}\left(\frac{x}{d_m^{\tau,NTS}}\right)^\gamma. \tag{21}$$

Integrating the inverse demand function between demands x_0 and x_1:

$$\int_{x_0}^{x_1} g_m^\tau(x).dx = \frac{\widetilde{C}_m^{\tau,NTS}}{\left(d_m^{\tau,NTS}\right)^\gamma}\int_{x_0}^{x_1} x^\gamma.dx = \frac{\widetilde{C}_m^{\tau,NTS}}{\left(d_m^{\tau,NTS}\right)^\gamma}\left[\frac{1}{\gamma+1}x^{\gamma+1}\right]_{x_0}^{x_1} = \frac{\widetilde{C}_m^{\tau,NTS}}{\left(d_m^{\tau,NTS}\right)^\gamma}\left(\frac{1}{\gamma+1}(x_1)^{\gamma+1} - \frac{1}{\gamma+1}(x_0)^{\gamma+1}\right).$$

Thus, integrating between the NTS demand and the elastic demand under toll setting $\boldsymbol{\omega}$, for each $m \in M$ and $\tau \in \Psi$, the Inverse Demand component of the social welfare objective function is:

$$Z_{ID}(\boldsymbol{t},\boldsymbol{f},\boldsymbol{\omega}) = \sum_{\tau\in\Psi}\sum_{m\in M}\int_{d_m^{\tau,NTS}}^{\bar{d}_m^\tau(\boldsymbol{t},\boldsymbol{f},\boldsymbol{\omega})} g_m^\tau(x).dx$$

$$= \sum_{\tau\in\Psi}\sum_{m\in M}\left\{\frac{\widetilde{C}_m^{\tau,NTS}}{(d_m^{\tau,NTS})^{\gamma}}\left(\frac{1}{\gamma+1}\left(\widetilde{d}_m^{\tau}(\boldsymbol{t},\boldsymbol{f},\boldsymbol{\omega})\right)^{\gamma+1}-\frac{1}{\gamma+1}(d_m^{\tau,NTS})^{\gamma+1}\right)\right\}, \tag{22}$$

where $\widetilde{d}_m^{\tau}$ is the elastic demand function in (9), for a given setting of the region travel times $\boldsymbol{t}$, regional path flows $\boldsymbol{f}$, and toll-prices $\boldsymbol{\omega}$. Note that the LoS under the NTS, $\widetilde{C}_m^{\tau,NTS}$, is different depending on whether departure time choice is being considered in the tolling scenario. If so, then the LoS in the NTS is calculated with regional path costs and probabilities from the traffic equilibrium with departure time choice (i.e. solving (19) with $\boldsymbol{\omega} = 0$). Otherwise, it is from the traffic equilibrium without departure time choice (i.e. solving (6) with $\boldsymbol{\omega} = 0$). Note though that $\widetilde{d}_m^{\tau}$ and $d_m^{\tau,NTS}$ remain the elastic demand and NTS demand before departure time choice is conducted. This is because the Inverse Demand component aims to capture only the costs incurred by travellers who have chosen not to travel by car. The costs incurred by departure time switchers are captured in the LoS component below. When $\boldsymbol{\omega} = 0$, $\widetilde{d}_m^{\tau} = d_m^{\tau,NTS}$, resulting in $Z_{ID}(0) = 0$.

The Level of Service component of Z_{SW} captures the disbenefit of tolling to the consumers (drivers) from increased travelling costs (or benefits from improved travel times). It is a surplus as it is relative to the costs they paid under the NTS. As discussed in Section 4, the LoS measure we adopt is the expected travel cost. Z_{LoS} is calculated as follows:

$$Z_{LoS}(\boldsymbol{t},\boldsymbol{f},\boldsymbol{\omega}) = \sum_{\tau\in\Psi}\sum_{m\in M} d_m^{\tau,NTS}\widetilde{C}_m^{\tau,NTS} - \sum_{\tau\in\Psi}\sum_{m\in M}\widetilde{d}_m^{\tau,DTC}(\boldsymbol{t},\boldsymbol{f},\boldsymbol{\omega}) \bullet \widetilde{C}_m^{\tau}(\boldsymbol{c}(\boldsymbol{t},\boldsymbol{f},\boldsymbol{\omega})), \tag{23}$$

where $\widetilde{d}_m^{\tau,DTC}$ is the departure time choice travel demand function in (18) and $\widetilde{C}_m^{\tau}$ is the LoS function in (8), given $\boldsymbol{t}, \boldsymbol{f}$, and $\boldsymbol{\omega}$. Note that when considering departure time choice, $d_m^{\tau,NTS}$ and $\widetilde{C}_m^{\tau,NTS}$ are based on the NTS traffic equilibrium with departure time choice (i.e. solving (19) with $\boldsymbol{\omega} = 0$). Otherwise, they are based on the NTS traffic equilibrium without departure time choice (i.e. solving (6) with $\boldsymbol{\omega} = 0$). Moreover, when not considering departure time choice, $\widetilde{d}_m^{\tau,DTC}$ is replaced with $\widetilde{d}_m^{\tau}$ in (9). When $\boldsymbol{\omega} = 0$, $\widetilde{d}_m^{\tau} = d_m^{\tau,NTS}$ and $\widetilde{C}_m^{\tau} = \widetilde{C}_m^{\tau,NTS}$, resulting in $Z_{LoS}(0) = 0$.

The Toll Revenue component of Z_{SW} captures the benefit of tolling for the governing authority who will receive the toll revenue. Z_{TR} is calculated as follows:

$$Z_{TR}(\boldsymbol{t},\boldsymbol{f},\boldsymbol{\omega}) = \sum_{\tau\in\Psi}\sum_{m\in M}\sum_{p\in P_m} f_{m,p}^{\tau}(\boldsymbol{\omega}) \bullet \mathrm{K}_{m,p}^{\tau}(\boldsymbol{t},\boldsymbol{f},\boldsymbol{\omega}), \tag{24}$$

where $f_{m,p}^{\tau}$ and $\mathrm{K}_{m,p}^{\tau}$ are the flow and toll paid on regional path $p \in P_m$ when departing during time-slice τ, given $\boldsymbol{t}, \boldsymbol{f}$, and $\boldsymbol{\omega}$. When $\boldsymbol{\omega} = 0$, there is no toll revenue, resulting in $Z_{TR}(0) = 0$.

Inserting (22) for Z_{ID}, (23) for Z_{LoS}, and (24) for Z_{TR} into (20), the full social welfare objective function is:

$$\begin{aligned} Z_{SW}(\boldsymbol{t},\boldsymbol{f},\boldsymbol{\omega}) &= Z_{ID}(\boldsymbol{t},\boldsymbol{f},\boldsymbol{\omega}) + Z_{LoS}(\boldsymbol{t},\boldsymbol{f},\boldsymbol{\omega}) + Z_{TR}(\boldsymbol{t},\boldsymbol{f},\boldsymbol{\omega}) \\ &= \sum_{\tau\in\Psi}\sum_{m\in M}\left\{\frac{\widetilde{C}_m^{\tau,NTS}}{(d_m^{\tau,NTS})^{\gamma}}\left(\frac{1}{\gamma+1}\left(\widetilde{d}_m^{\tau}(\boldsymbol{t},\boldsymbol{f},\boldsymbol{\omega})\right)^{\gamma+1}-\frac{1}{\gamma+1}(d_m^{\tau,NTS})^{\gamma+1}\right)\right\} \\ &+\left(\sum_{\tau\in\Psi}\sum_{m\in M} d_m^{\tau,NTS}\widetilde{C}_{m,p}^{\tau,NTS} - \sum_{\tau\in\Psi}\sum_{m\in M}\widetilde{d}_m^{\tau}(\boldsymbol{t},\boldsymbol{f},\boldsymbol{\omega}) \bullet \widetilde{C}_m^{\tau}(\boldsymbol{c}(\boldsymbol{t},\boldsymbol{f},\boldsymbol{\omega}))\right) \\ &+\sum_{\tau\in\Psi}\sum_{m\in M}\sum_{p\in P_m} f_{m,p}^{\tau} \bullet \mathrm{K}_{m,p}^{\tau}(\boldsymbol{t},\boldsymbol{f},\boldsymbol{\omega}). \end{aligned} \tag{25}$$

The toll-price optimisation problem is therefore:

$$\max_{\boldsymbol{\omega}} \; Z_{SW}(\boldsymbol{t},\boldsymbol{f},\boldsymbol{\omega}) \tag{26}$$

subject to :

$$\boldsymbol{t} = \boldsymbol{H}(\boldsymbol{t},\boldsymbol{f}) \tag{27}$$

$$\boldsymbol{f} = \widetilde{\boldsymbol{d}}^{DTC}(\boldsymbol{t},\boldsymbol{f},\boldsymbol{\omega}) \bullet \boldsymbol{Q}(\boldsymbol{c}(\boldsymbol{t},\boldsymbol{f},\boldsymbol{\omega})) \tag{28}$$

$$\boldsymbol{\omega} \geq 0 \tag{29}$$

Constraint (27) is the traffic propagation region travel time fixed-point problem, see Section 2.2. Constraint (28) is the D-MR-MFD-SUE with elastic demand and departure time choice regional path flow fixed-point problem in (19), which for simplicity of notation has been vectorised. This constraint can be replaced with the appropriate traffic equilibrium depending on whether elastic demand and departure time choice are or are not being considered. Constraint (29) stipulates that the toll-prices should be non-negative.

Note that in (25), as is typically done, it is assumed that the disbenefit to the consumer and benefit to the producer of a toll have equal worth for society, and so the tolls paid and received cancel out. This is a very classical assumption that is made, however it need not be true, as it depends on how the tolls received are reinvested to benefit consumers. It could be that the toll revenues are not fully reinvested (e.g. if there is a private operator that is remunerated for the operation, or if there are multiple authorities with different jurisdictions), or do not benefit society in an equivalent manner to the disbenefit from paying the tolls. To account for this one could scale the producer component of the social welfare objective function by a scaling factor between 0 and 1. In Appendix B we explore how results differ in the real-life case study for different values of this scaling factor.

As described above, when the tolls are zero ($\boldsymbol{\omega} = 0$), the objective function equals zero. For a given setting of the tolls $\boldsymbol{\omega}$, the dynamic multi-region MFD SUE traffic model is re-solved, outputting equilibrated regional path flows and region travel times to update the objective function. The objective function surface will not be globally concave, since as the toll-price tends to infinity there will be an inertia, where demand can no longer change their regional path or departure time to avoid paying a toll, or there is no longer any car demand. Ideally, the objective function surface will be smooth and have a unique maximum. In each case, we check this by manually inspecting the objective function by performing a grid search and plotting the surface. In the cases studied, we have found the objective function to be smooth and have a unique maximum (see Fig. 11D, Fig. 20, & Fig. 26B). Thus, although we cannot mathematically prove that the toll-prices we identify are optimal, we provide empirical evidence to support that they are.

5.2. Demonstration

To demonstrate, consider the example multi-region MFD system in Fig. 3. Fig. 11A–C plot how the Inverse Demand, LoS, and Toll Revenue components of the social welfare objective function vary as the toll-price is varied, for different configurations of the dynamic multi-region MFD SUE model: Fixed Demand (FD) with and without Departure Time Choice (DTC) and Elastic Demand (ED) with and without DTC. The regional path choice model parameters are as in Section 3.1, and the elastic demand and departure time choice parameters are $\gamma = 0.7$ and $\mu = 3$, respectively (the same as for Fig. 8C).

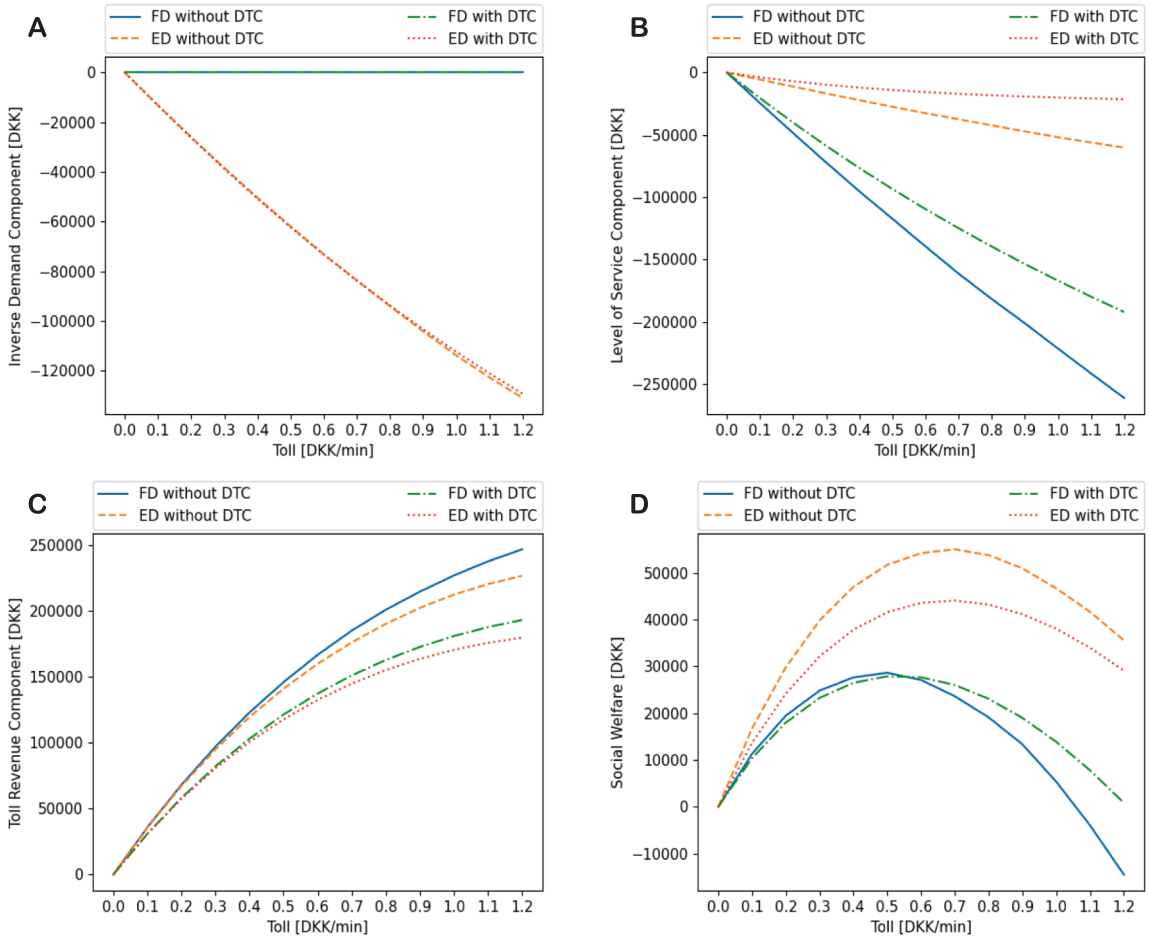

Fig. 11. Example system: Objective function components as toll-price is varied, for fixed/elastic demand with/without departure time choice. A: Inverse Demand component. B: Level of Service component. C: Toll Revenue component. D: Social Welfare.

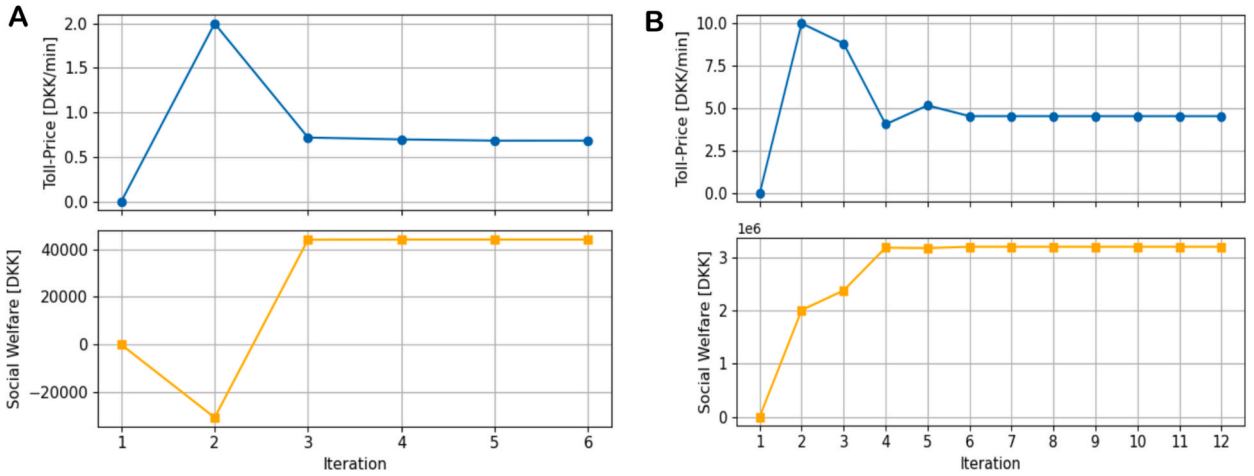

Fig. 12. Demonstrating convergence of the adopted optimisation algorithm for maximising social welfare. A: Example system. B: Real-life case study.

As shown in Fig. 11A, with fixed demand the Inverse Demand component is always zero. With elastic demand, the Inverse Demand components decrease with the toll price, as more people shift away from car due to increased costs of travelling. The Inverse Demand component estimates the costs experienced from not travelling by car, for example the LoS of taking a different mode or cost of cancelling.

As shown in Fig. 11B, the LoS component decreases much faster for fixed demand than elastic demand. This is because with elastic demand the demand decreases as the toll-price increases, resulting in lower total car traveller costs experienced (as there are fewer car travellers), as well as quicker travel times for these car travellers from lower congestion levels.

As shown in Fig. 11C, the Toll Revenue component for each model increases as the toll-price increases, as one would expect. It increases slower for elastic demand as the lower demand levels mean less tolls received.

Fig. 11D plots how the social welfare objective function varies as the toll-price varies, for the different models. As shown, the objective functions have a unique maximum in this range of the toll-price. For the fixed demand models, welfare increases initially as flow is pushed onto the non-tolled r-path and thus the travel time of the congested tolled r-path decreases. Increasing the toll-price too much, however, leads to too much flow taking the longer non-tolled r-path resulting in a decrease in welfare. For the departure time choice models, tolling instigates a beneficial shift to departing earlier/later, which initially alleviates congestion during peak hours, but then as the toll-price increases this results in displacing congestion to the off-peak period. For the elastic demand models, the higher the toll-price the lower the demand level and thus the lower the travel times for both r-paths. However, as more people opt not to travel by car, the total cost incurred for those travellers increases, which at some point outweighs the saved cost from improved travel times for the car travellers.

The fixed demand optimised toll-prices are lower than the elastic demand optimised toll-prices. This is because, for elastic demand, the lower travelling costs for remaining car travellers through travel time savings from the decreased demand, outweigh the costs for the travellers who choose not to travel by car.

5.3. Optimisation solution methodology

Algorithm 2 outlines general pseudo-code for solving the toll-price optimisation problem. In this study, to identify the toll-prices to test in the next iteration in Step 3, we applied a convex minimisation algorithm (minimising $-Z_{SW}$). Since the derivative of the objective function cannot be calculated analytically, we approximated the gradient using finite difference. This was operationalised through applying the L-BFGS-B bound-constraint, quasi-Newton minimisation algorithm (Byrd et al., 1995). As discussed in Section 5.1 above, to check the validity of using convex minimisation, we also manually inspected the objective function surface, which we found, in those cases, to have a unique maximum and be locally concave in the reasonable range of toll-prices evaluated (see Fig. 11D / Fig. 12).

Algorithm 2. Pseudo-code for solving the toll-price optimisation problem.

Step 0: *Initialisation.* Initialise the toll-price vector $\boldsymbol{\omega}^{(0)}$ for iteration $k = 0$. Set $k = 1$.

Step 1: *Re-solve the dynamic multi-region MFD SUE traffic model.* Given the toll-price vector $\boldsymbol{\omega}^{(k)}$ for iteration k, re-solve the dynamic multi-region MFD SUE traffic model (see Section 4.2) to obtain the equilibrated regional path flow vector $\boldsymbol{f}^{*,(k)}$ and equilibrated region travel time vector $\boldsymbol{t}^{*,(k)}$ for iteration k.

Step 2: *Compute social welfare objective function.* Given the equilibrated regional path flow vector $\boldsymbol{f}^{*,(k)}$ and equilibrated region travel time vector $\boldsymbol{t}^{*,(k)}$ obtained in the previous step, compute the social welfare objective function $Z_{SW}^{(k)}$ for iteration k (see Eq. (25)).

(*continued on next page*)

(*continued*)

Algorithm 2. Pseudo-code for solving the toll-price optimisation problem.

Step 3: *Identify toll-price search direction.* Based on $Z_{SW}^{(s)}$ and associated toll-price vectors $\boldsymbol{\omega}^{(s)}$ for all $s \leq k$, identify a new set of toll-prices $\boldsymbol{\omega}^{(k+1)}$ to test in the next iteration $k+1$.

Step 4: *Check for convergence.* If social welfare objective function and toll-prices have sufficiently converged, stop. Otherwise, set $k = k+1$ and return to Step 1.

To demonstrate the toll-price optimisation solution method, Fig. 12A–B display for the small-scale example multi-region MFD system in Fig. 3 and real-life case study (see Sections 6 & 7), respectively, the toll-price and social welfare objective function values at each iteration of the L-BFGS-B algorithm, solving with the D-MR-MFD-SUE with elastic demand and departure time choice model. For the example system the model specifications are the same as those for Fig. 8C/Fig. 11, and for the real-life case study the model specifications are as discussed in Section 6.2. For both cases the initial toll-price condition was set as 0 DKK/min, while the bound-constraints for the algorithm were set as $[0, 2]$ for the example system and $[0, 10]$ for the real-life case study. As shown, in both cases, the algorithm successfully identifies the toll-price that maximises social welfare. For the example system, the optimised toll-price of 0.684 DKK/min aligns with the visual social welfare maximum in Fig. 11D (see the red dotted curve). For the real-life case study, the optimised toll-price of 4.544 DKK/min aligns with the visual social welfare maximum in Fig. 20.

In the cases studied in this paper, we only optimise a single toll-price, but multiple toll-prices can be optimised. In Appendix C we demonstrate the model / algorithm optimising multiple toll-prices.

6. Case study setup

6.1. Multi-region MFD system

We shall briefly provide details here on the case-study multi-region MFD system and how it was set-up. For an in-detail description of the system and how it was set-up see Section 5 in Duncan et al. (2025).

The area of the case study is large, spanning eastern Zealand in Denmark, as depicted in Fig. 13. The area includes the urban area cities/towns of Copenhagen, Roskilde, Hillerød, and Helsingør, as well as rural areas between the cities/towns. There is also a motorway network superimposed upon the rural and urban areas, as well as external entry/exit points (port zones) to the area. First, 39 urban/rural underlying regions were partitioned by grouping together several neighbouring administrative zones ('GMM' zones) using

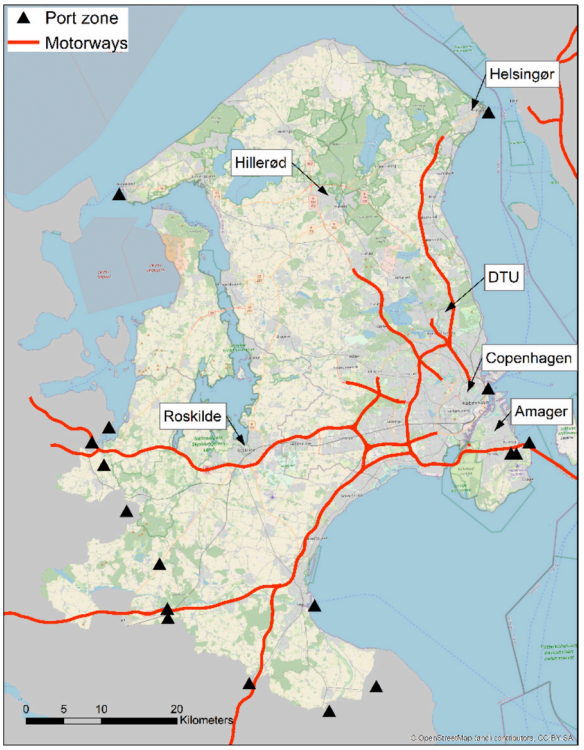

Fig. 13. Area of case study.

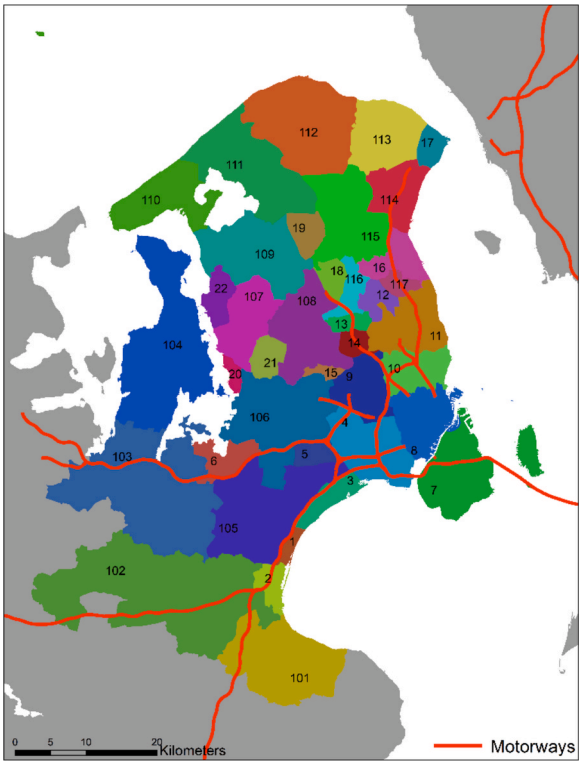

Fig. 14. Underlying region partitioning and superimposed motorway network.

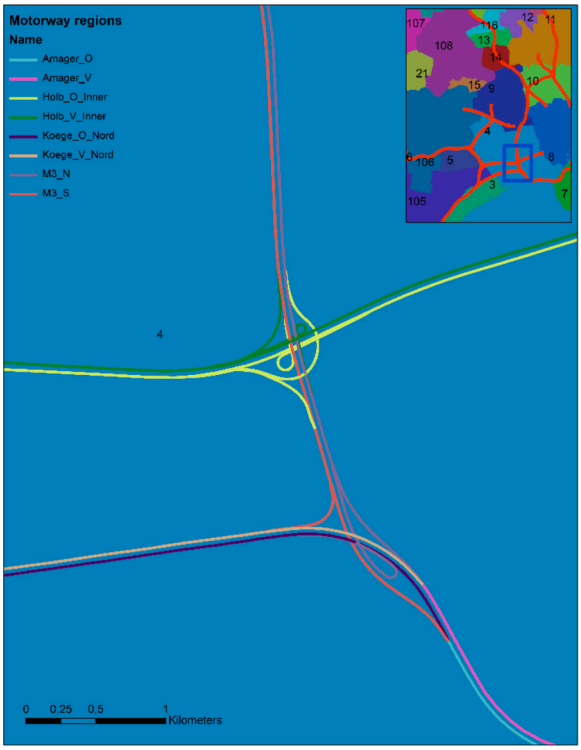

Fig. 15. Example of superimposed motorway region partitioning.

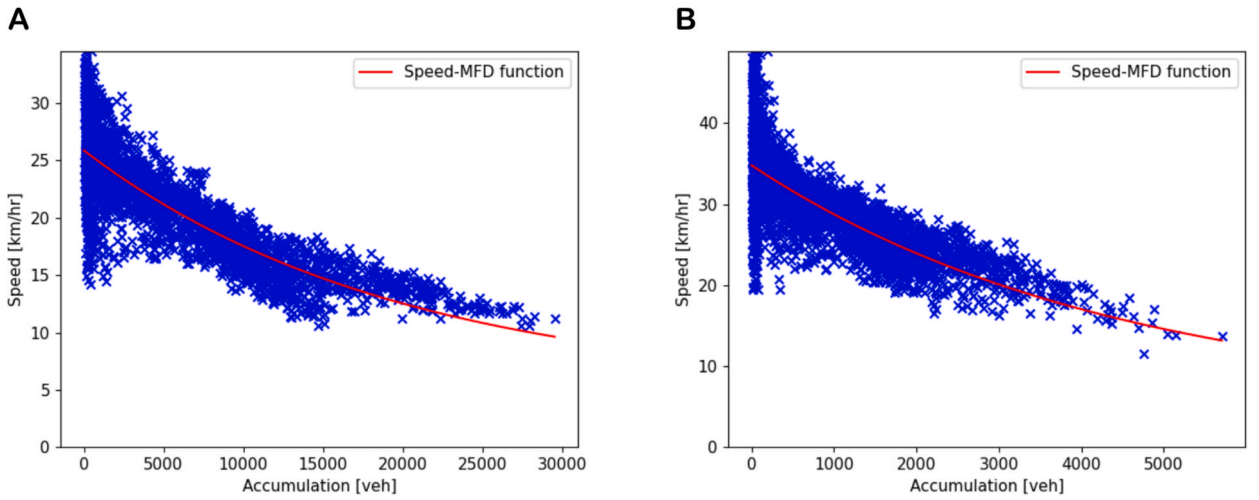

Fig. 16. Examples of two fitted exponential speed-MFD functions. A: Region 8 – Greater Copenhagen. B: Region 7 – Amager.

logic, local understanding, and trial-and-error, see Fig. 14. Then, 96 superimposed motorway regions were partitioned according to the underlying regions, and then further by name, direction, and at junctions, as exemplified in Fig. 15. There are thus 135 regions in total, where both the underlying regions and motorways regions are treated as regions the same in the system, though with different speed-MFD functional forms, see below.

The speed-MFD functions for each of the regions were calibrated using a combination of probe vehicle data and vehicle count data, the latter being used to estimate the penetration rate of the probe vehicles (= 3.84 %). Speed-MFD functional forms were fitted to a set of cleaned accumulation-speed datapoints. For the underlying urban/rural regions, we fit an exponential speed-MFD functional form. This is as follows for an accumulation state n_r:

$$v_r(n_r) = (a-h)e^{-bn_r} + h,$$

where $a > 0$ gives the free-flow region speed, $b > 0$ determines the curve of the speed function, and h is the minimum speed. Fig. 16 plots two examples.

For the motorway regions, we fitted a piecewise-exponential speed-MFD functional form. This is as follows for an accumulation state n_r:

$$v_r(n_r) = \begin{cases} (a-h)e^{-bn_r} + h & \text{if } n_r \le n_r^{crit} \\ (a-h)e^{-bn_r^{crit}} e^{-c\left(n_r - n_r^{crit}\right)} + h & \text{if } n_r > n_r^{crit} \end{cases},$$

where $a > 0$ gives the free-flow region speed, $n_r^{crit} > 0$ is the critical accumulation, $b > 0$ and $c > 0$ determine the curves of the speed function pre- and post-critical accumulation, respectively, and h is the minimum speed. Fig. 17 plots two examples.

As described above, each underlying region is associated with a set of administrative GMM zones. The indexed set of regional OD movements M was determined by considering whether for each pair of origin and destination region, any demand is travelled across the day from any GMM zone in the origin region to any GMM zone in the destination region. Due to the presence of external entry/exit points (port zones) (see Fig. 13), an underlying region can have more than one origin/destination point, i.e. internal and external. Regional OD movement $1 \in M$ could for example be from external origin in region 17 (flow entering from the Helsingør ferry from Sweden) to internal destination in region 6 (Roskilde). There are in total 1898 regional OD movements.

The regional OD movement travel demands were obtained by aggregating the travel demand from all GMM zones in the origin region to all GMM zones in the destination region. Fig. 18 plots the total travel demand across the OD movements at each 30-min time-slice of the day. As shown, there are two demand peaks, in the morning and evening, as one would expect.

To obtain the regional path choice sets, shortest path searches were conducted between GMM zones of regional OD movements on the actual link-network, based on different link travel costs, to identify a set of link-routes for each regional OD movement. The regional path of each link-route was obtained by tracing along it and determining the order of regions it traverses. The unique generated regional paths for each regional OD movement were then determined. To obtain reasonably-sized regional path choice sets, the choice sets were trimmed, in a manner maximising the variation in r-paths. See Algorithm 2 in Duncan et al (2025) for details on the entire process. The maximum choice set size was 23 and the total number of r-paths is 31,760.[3] The lengths of the links in the

[3] Note that we have extended the regional path choice sets in Duncan et al. (2025) for regional OD movements where there were regional paths passing through the tolled regions (see Fig. 19), but none avoiding the tolled regions. We did this by setting very large link costs for the links inside the tolled regions and conducting shortest path searches based on different link costs. A maximum of three extra regional paths were added.

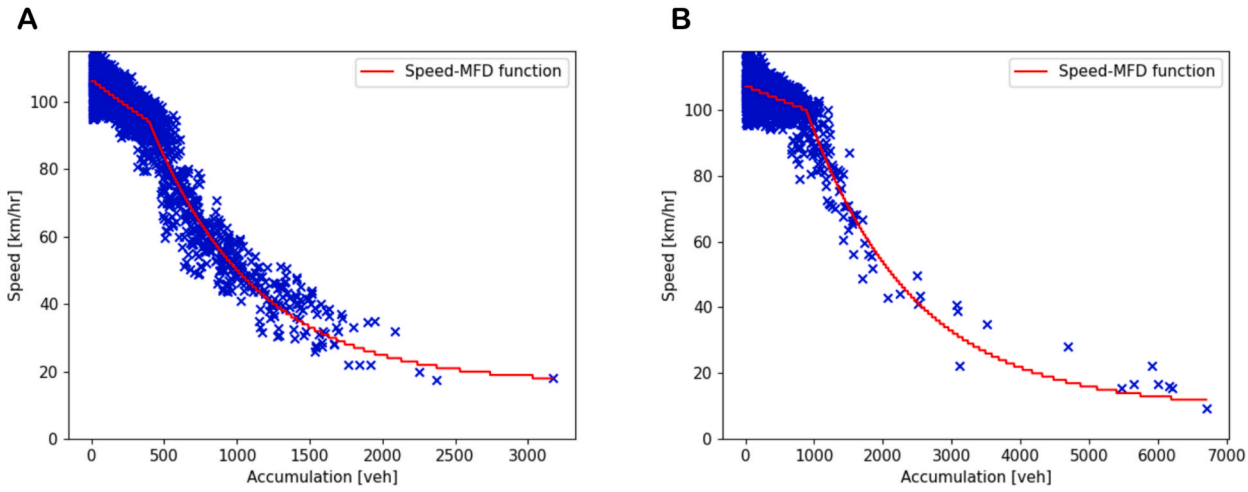

Fig. 17. Examples of two fitted piecewise-exponential speed-MFD functions. A: Region 10 motorway 'M3_N'. B: Region 11 motorway 'Hels_N'.

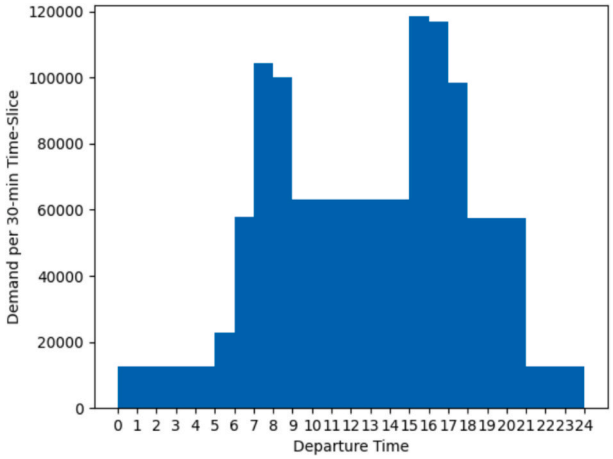

Fig. 18. Total travel demand across regional OD movements at each 30-min time-slice of the day.

generated link-routes for each regional path were used to determine the average regional trip lengths of each region in each regional path.

6.2. *Model specification*

For the case study, we obtained model parameter values by assuming a VOD value and fitting the other model parameters to data. The assumed VOD value was obtained from the official Danish transport economic unit price catalogue (Transportministeriet, 2024). Assuming that perceived distance costs to drivers are associated with perceived petrol costs and maintenance costs, then the VOD is $\alpha_l = 0.96$ [DKK/km]. We then estimated the other parameters of the dynamic multi-region MFD SUE model, utilising the same procedure and dataset described in Duncan et al. (2025). We estimated VOT by setting $\alpha_{tt} = \frac{\alpha_l}{\alpha_{l/tt}}$, where α_l is the VOD and $\alpha_{l/tt}$ is a parameter estimated describing the relative preference of travel time compared to length. We therefore estimated three parameters: $\alpha_{l/tt}$, the C-Logit scaling parameter θ, and the C-Logit commonality scaling parameter ν (like we did in Duncan et al. (2025)). The parameter estimates we obtained were $\widetilde{\theta} = 0.0658$, $\widetilde{\nu} = 0.1389$, and $\widetilde{\alpha}_{l/tt} = 0.4827$, the latter implying that travellers are prepared to drive around 2 km further to save 1 min of travel time, which is a reasonable result. The VOT is thus $\alpha_{tt} = \frac{0.96}{0.4827} = 1.99$ [DKK/min]. For the car demand elasticity parameter, we assumed a value of $\gamma = 0.2$, taken from values used in the Danish national transport model (see Rich & Hansen, 2016), but also corroborated with values from other studies. For the departure time choice Logit scaling parameter, we assumed a value of $\mu = 2$, determined through manual experimentation, balancing sensitivity to changes in departure time-slice utilities (e.g. with tolls) against reproducing the original demand profile. In Appendix D we provide an overview of all the parameters we specify in the case study, as well as the data sources / studies used to determine their settings.

The tolled regions are regions 3, 4, 7, 8, 9, & 10, see Fig. 19. Region 8 is the region of central Copenhagen and the other regions are

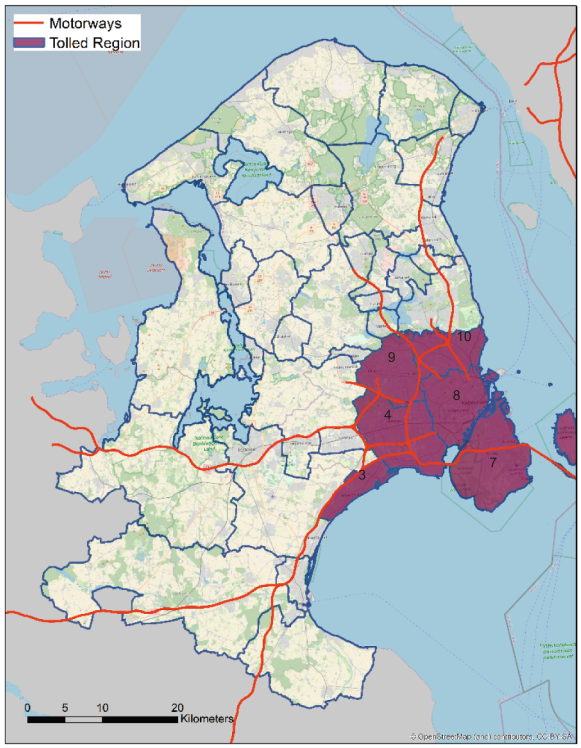

Fig. 19. Tolled area of case study.

the surrounding urban areas (see Fig. 13 / Fig. 14). The time-based toll is enforced between 7 and 9am and 3–6 pm, i.e. the morning and evening peaks. A single toll-price is optimised for each of the tolled regions and tolled time-slices. These specifications were chosen as these are the specifications being considered by the Danish government.

Note that, for the reasons discussed/demonstrated in more detail in Sections 6.2.2 & 6.2.3 in Duncan et al. (2025), for the regional path choice, travel costs in the origin and destination regions are disregarded. This is because the regional path choice we are trying to capture is from a general point (e.g. a centroid) in the origin/destination regions, and including the origin/destination region costs may misrepresent choice behaviour. This was supported empirically, where it was found that basing regional path choice on travel costs excluding origin/destination costs provided considerably better fit to the data than including them.

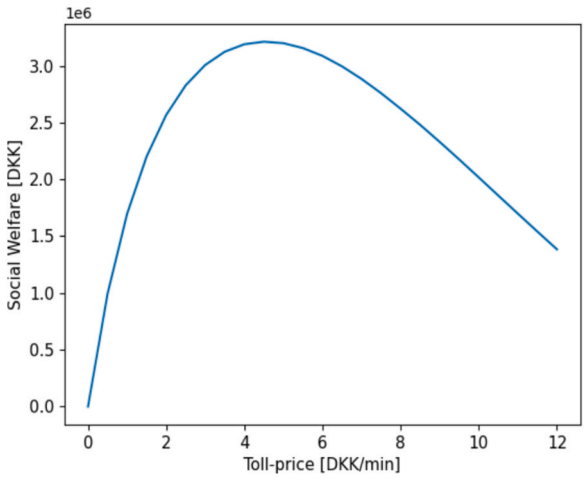

Fig. 20. Real-life case study: Social welfare objective function surface for the dynamic multi-region MFD SUE model with elastic demand and departure time choice.

Table 1
Optimal toll price and gain in social welfare.

Optimal toll-price	Daily gain in social welfare from NTS	Percentage daily gain in social welfare from NTS	Daily welfare gain per capita	Net benefit to revenue ratio
4.544 DKK/min	3,212,034 DKK	2.12 %	1.26 DKK/veh	0.10

7. Case study results

For the case study, we shall focus on the results for the full D-MR-MFD-SUE model with elastic demand and departure time choice. Fig. 20 displays the social welfare objective function surface, and Table 1 displays the optimal toll-price, along with different measures of the predicted social welfare gain. As can be seen, the objective function is smooth and has a unique maximum. To put the optimal toll-price into perspective, 4.544 DKK/min corresponds to around 0.52 £/min, 0.7 $/min, and 0.61 €/min. Thus, a 20-minute trip through the tolled area during the tolling period would cost around £10. The optimal toll-price is thus not unreasonable, though it is perhaps a little high. We shall discuss potential reasons for this later.

In terms of the predicted social welfare gains, the net benefit to revenue ratio (daily gain in social welfare divided by total daily revenues) of 0.10 is a comparable order of magnitude to some other studies, with Eliasson and Mattsson (2006), de Palma et al. (2005), and Jing et al. (2024) finding values of 0.32, 0.28, and 0.11–0.3, respectively. Moreover, it is similar to the ratio found in an old study of a similar tolling scheme in Copenhagen in Rich & Nielsen (2007). Excluding the system costs (as we do), they find a net benefit to revenue ratio of 0.12 for the distance-based scheme, similar to our 0.10. The fact that our ratio is at the lower end of these could be explained by the fact that that our social welfare function does not currently consider any other externalities such as benefits from reduced emissions, noise, and accidents, unlike most of these studies. Jing et al. (2024) find a daily welfare gain per capita ranging between 0.26 and 3.53 DKK/person depending on the tolling scheme, which sits our 1.26 DKK/veh within the range. The fact that our value is at the lower end might be expected given that many travellers in our case study area are not affected or are only minorly affected due to travelling in areas away from the tolled regions (approximately 25%).

Regarding the main purpose of the tolling, in reducing congestion in the main area of Copenhagen, the optimal tolling scheme results in a 7.17% reduction in total vehicle-kilometres driven in the tolled regions. Benchmarking with the reductions found in Rich and Nielsen (2007), they found a 6.7% reduction in the total vehicle-kilometres driven in the county of Copenhagen, which is not a one-to-one match with our tolled area, but somewhat similar. During the tolled hours, our study found a 28.63% reduction in vehicle-kilometres in Copenhagen, leading to higher speeds. On average, drivers travel 0.91 km/hr faster in the tolled underlying urban regions during the tolled hours, and in some places 4.02 km/hr faster. For the tolled motorway regions, drivers travel on average 7.87 km/hr faster, and in some places 50.67 km/hr faster. Hence, there is a clear alleviation in congestion in the main area of Copenhagen.

We shall now explore the effects of tolling on travel behaviour, considering in turn the effects of tolling on regional path choice, elastic demand, and departure time choice.

Regional path choice

While 68.7% of travel demand has a regional path option for their OD movement that travels in the tolled area (which is the main area of Copenhagen), 58.8% of demand originates and/or destinates in the tolled regions. For these OD movements, drivers cannot change their regional path to avoid experiencing a toll. They can maybe choose a regional path that travels less time in the tolled regions, but they cannot avoid paying a toll. The main impact of tolling on regional path choice is for OD movements that do not originate or destinate in the tolled regions, but have a regional path that passes through a tolled region. This is 9.8 % of the travel demand. Under the NTS, 2.75 % of demand passes through the tolled regions, whereas under the optimal tolling scenario this figure decreases to 2.29%.[4] This indicates that tolling will have some impact on regional path choice, with the impact being to divert travellers to going around the main Copenhagen area.

To demonstrate, Fig. 21 displays two regional paths from the external origin of region 101 to the external destination of region 17 (i.e. from the far south of the study area to far north). R-path 1 (the orange r-path) goes through the tolled regions on motorways and r-path 2 (the green r-path) goes around the tolled regions on minor roads. Fig. 22A displays the travel times for these two regional paths when departing at different times across the day. Fig. 22B displays their choice probabilities. As can be seen, under the NTS r-path 1 is much quicker than r-path 2, and thus r-path 1 has a higher choice probability than r-path 2. The travel time for r-path 1 worsens during the peak hours, but it remains quicker. Under the optimal tolling scenario the congestion levels are lower in the tolled area, and thus r-path 1 travel times are less during the peak hours than under the NTS. R-path 1 travellers, however, have to pay a toll, which results in r-path 1 overall having a higher travel cost (than under the NTS). This results in an increase in travellers taking r-path 2 during the peak hours.

Elastic demand

In the optimal tolling scenario, there is a 3.55% decrease in the total demand travelling by car from the NTS. This figure roughly aligns with

[4] Note that in the tolling scenario this is of the demand continuing to travel by car.

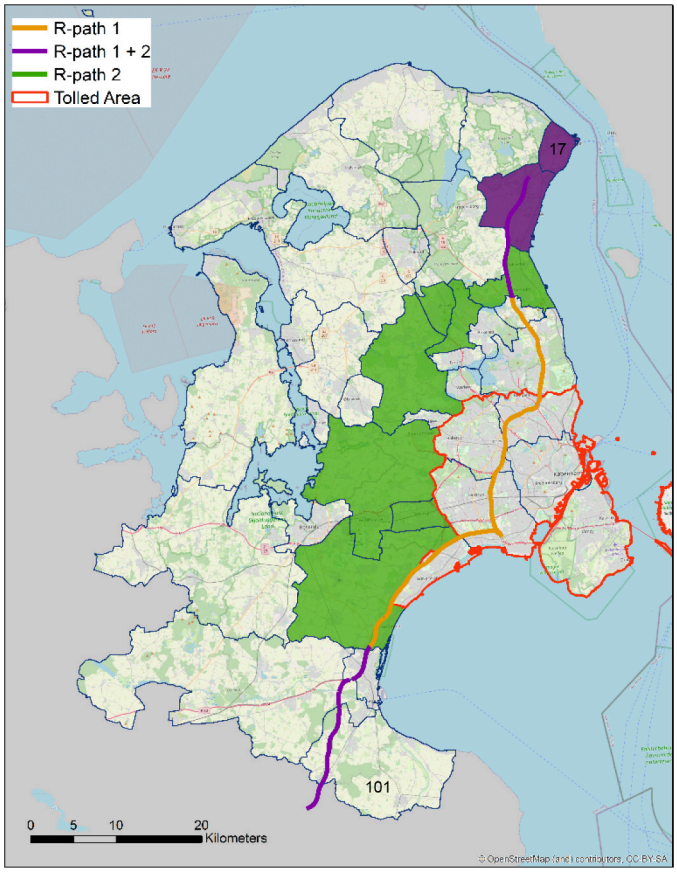

Fig. 21. Real-life case study. Two regional paths from the external origin of region 101 to the external destination of region 17 (from very south to very north), one passing through the tolled area and one going around.

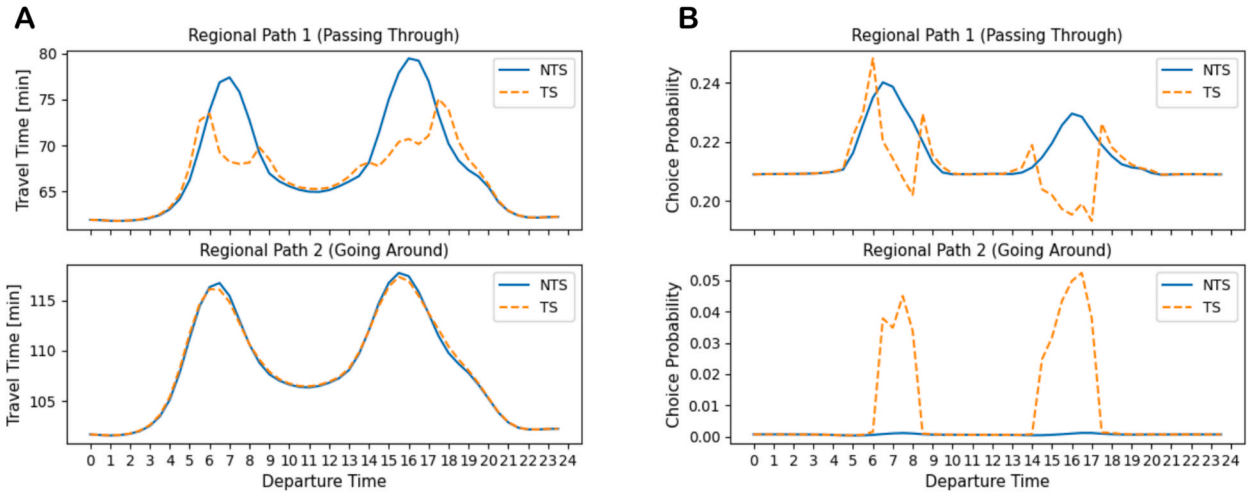

Fig. 22. Real-life case study. Travel times (A) and choice probabilities (B) for the two regional paths in Fig. 21 when departing at different times across the day, under the NTS and optimal tolling scenario.

the findings in Rich & Nielsen (2007), who predict a 1.6–7.5% decrease in total car demand from tolling in Copenhagen, depending on the scheme. When inspecting the percentage decrease in demand during the peak hours, the number is higher. Fig. 23A displays, for the OD movements that have a regional path travelling in the tolled regions, the average percentage difference in LoS across the day between the NTS and the optimal tolling scenario. Fig. 23B displays the percentage difference in demand, before departure time choice (i.e. just the

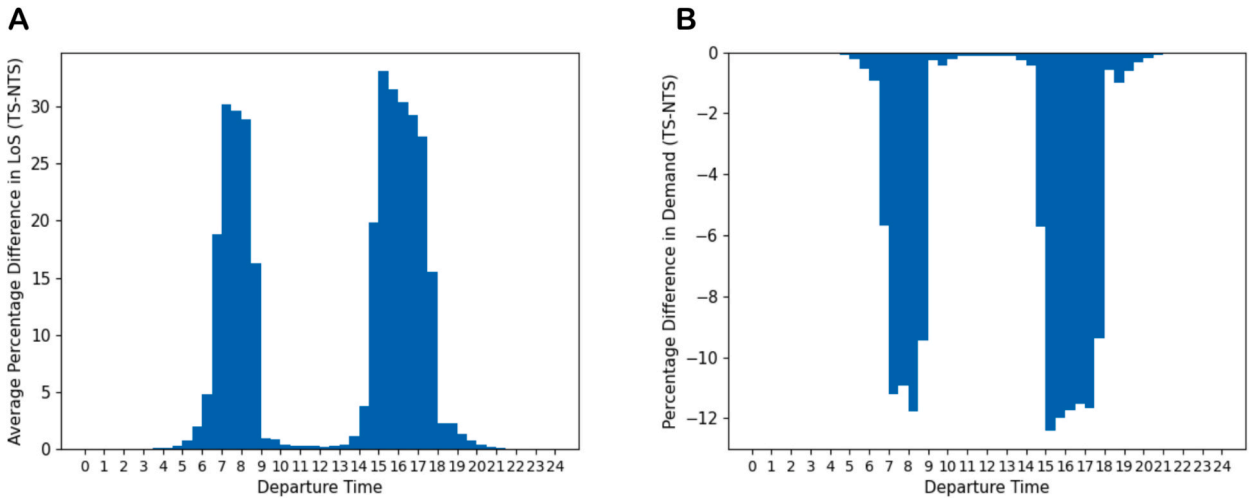

Fig. 23. Real-life case study. A: Average percentage difference in LoS across the day between the NTS and optimal tolling scenario (positive number means worse LoS in the optimal tolling scenario). B: Percentage difference in the travel demand (negative number means less demand in the optimal tolling scenario).

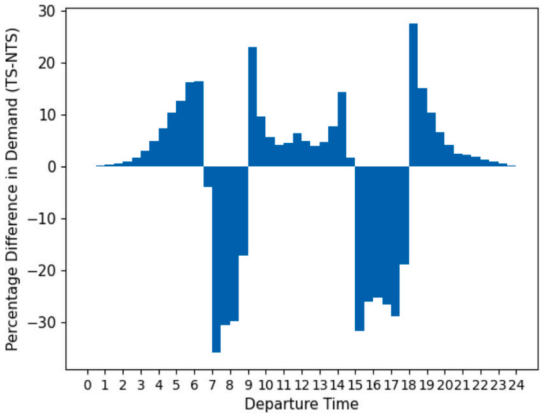

Fig. 24. Real-life case study. Percentage difference in travel demand across the day between the NTS and the optimal tolling scenario, for OD movements that have a regional path entering the tolling area.

difference in demand from the elastic demand component of the model). As shown, during and around the peak hours, the LoS worsens on average by up to around 30%, which results in around a 12% decrease in travellers travelling by car. This is also perhaps a bit low, which could be because the demand elasticity parameter for car is a bit low, or it could be because changing departure time is a better option, which we explore next.

Departure time choice

Fig. 24 displays, for the OD movements that have a regional path travelling in the tolled regions, the percentage difference in demand across the day between the NTS and the optimal tolling scenario. As can be seen, tolling instigates a clear shift in departure choice, with many opting to depart earlier or later than the tolling period to avoid/reduce paying a toll. Noting that the percentage changes in the figure include those opting not to travel by car at all, then this would infer around 20% of travellers usually departing during the peak hours opt to depart earlier or later. It therefore appears that the most prominent action travellers take to avoid/decrease paying a toll is to change their departure time. This could though in this case study be because only a small proportion of travellers pass through the tolled regions under the NTS (2.7%), and therefore not many travellers can change their regional path to avoid tolling. And/or because the assumed demand elasticity parameter for car is a little low, underestimating the number of drivers that will opt not to travel by car.

As mentioned above, the toll-price is perhaps a little high. There are several potential causes for this, four of which are as follows. The first cause could be the tolling setup. The tolled regions cover the main urban area of Copenhagen, which as can be seen in Fig. 19 is located to the east of Zealand against the sea. Most of the traffic that passes through the tolled area is travelling between the

north (e.g. Helsingør, Hillerød (see Fig. 13)) and the south/south-west (e.g. Roskilde / the motorways heading west/south). The quickest routes connecting the north and south/south-west are on the motorways, which all pass through the tolled area. Avoiding the tolled area means travelling on more minor roads, which takes longer. There will thus be some reluctance of travellers that usually pass through the tolled regions to go around. Our intuition is that a fairly high toll-price will be required to push travellers onto the minor roads travelling around the tolled regions, but a toll-price of 4.544 DKK/min is perhaps a little high.

A second cause could be that the estimated θ Logit scaling parameter for the C-Logit regional path choice model is low. A larger value of θ would push travellers onto the regional paths going around the tolled regions at a faster rate as the toll-price is increased. Analysing this, we optimised the toll-price with the θ parameter set to three times its calibrated value, i.e. $\theta = 3 \times 0.0658 = 0.1974$. The new optimal toll-price was 4.334 DKK/min, so only slightly lower than the original 4.544 DKK/min toll-price. This is likely because, as discussed above, only a small proportion of travellers pass through the tolled regions under the NTS (2.7%), and therefore not many travellers can change their regional path to avoid tolling. The main action that travellers take is to change their departure time, and perhaps due to this, changing regional path is less required.

A third cause could be that the costs for not travelling by car inferred from the inverse demand function are lower than one would expect. The elastic demand function predicts, for a given increase in car travelling costs, how many travellers will opt not to travel by car. The inverse demand function thus predicts, for a given number of travellers that have opted not to travel by car, the increased car travelling costs that will have instigated such a demand decrease. These are the costs that travellers are assumed to experience from not travelling by car, but these could well be underestimating the true mode switch / trip cancellation costs. If the non-car travelling costs were higher, and the same number of travellers choose not to travel by car, social welfare would decrease. For example, when optimising the toll-price with the Inverse Demand component scaled by 1.25, i.e. the costs of not travelling by car are 25% greater, the optimal toll-price is 3.173 DKK/min, 1.371 DKK/min less than the original 4.544 DKK/min.

8. Conclusions and future research

This study has extended the dynamic multi-region Macroscopic Fundamental Diagram (MFD) Stochastic User Equilibrium (SUE) model introduced in Duncan et al. (2025) to account for elastic demand and departure time choice, and then integrated the model within a time-based toll-price optimisation framework for maximising social welfare. In both a simple example multi-region system and a real-life case study we have shown that the modelling and optimisation framework provides a computationally tractable approach to optimising toll prices, which yield welfare gains and desirable behaviour changes.

While the developed tolling model is a very promising approach, there are several aspects that require further consideration.

Calibration of model parameters. Calibration of the regional path choice model parameters requires careful consideration. For the case study in this paper, we have taken a reasonable Value of Distance (VOD) value from an official Danish unit price study, and calibrated the other parameters according to observed behaviour under the No Tolling Scenario (NTS). We have found that this yields a reasonable Value of Time (VOT) value, and represents behaviour reasonably in the NTS. However, as we do not have available data to calibrate the sensitivity of travellers to tolls, we have assumed that travellers' sensitivity to monetary toll is the same as their sensitivity to the assumed monetary cost of travel distance and time. Studies have found though that travellers can be quite sensitive to having to pay tolls, and thus our assumption is perhaps underrepresenting travellers' sensitivity. Further research could therefore try to explicitly calibrate travellers' sensitivity to toll, perhaps through a stated preference survey, or a trial tolling experiment, which is currently being conducted in Denmark.

Non-car travelling costs. To predict how travellers will opt not to travel by car due to tolls, we have adopted a traditional elastic demand approach, where the Inverse Demand function predicts the costs incurred from opting not to travel by car. It is convenient as it does not need to know the costs of the alternative options to travelling by car, but that is also its limitation. Ideally, the car tolling model would be paired with a mode choice model, to contrast the increased car travelling costs from tolls with the costs for instead travelling by public transport, bicycle, or other modes. This would more accurately capture travellers' inclination to mode switch, and the costs of doing so. This is something we hope to explore in future research.

Heterogeneity of preferences. In this study, we have assumed all travellers have the same preferences. Different travellers / trip types may, however, have different preferences. For example, wealthy travellers may have a high VOT and low sensitivity to toll, while leisure trips may have a lower VOT and lower arriving late penalty. This is likely to have an impact on the optimal toll price, which further research could explore.

Marginal cost of public funds. The marginal cost of public funds is defined as "the factor by which the marginal resource cost of a public project should be scaled to take into account that the project is financed through distortionary taxation" (Eliasson, 2009). In this study, as is typically done, we have assumed that this factor is equal to 1. The marginal cost of public funds is however often supposed to be greater than 1. In Sweden for example it is generally taken to be 1.3 (Hansson, 1985; Eliasson, 2009). Further research could explore results when taking the marginal cost of public funds into account in the social welfare objective function. And/or considering different redistribution of revenue policies such as equity schemes, assessing their impact on behaviour and optimal toll price.

Future research also includes integration within a car ownership model, properly calibrating a departure time choice model in the case study, evaluating different tolling schemes (e.g. distance-based, fixed price), and considering other externalities within the social welfare function such as emissions, noise pollution, and reduced accidents (Rich & Nielsen, 2007). It would also be interesting to explore how the results from toll optimisation with the aggregate region-based traffic model in this study compares with results from a transport simulation model such as Matsim. The detail in these models allows responses to tolls to be captured with a high level of realism, and therefore it would be useful to validate our approach by comparing with these models. Beyond toll-price optimisation, one could use the traffic model to explore other policy schemes, such as behaviour changes / emissions under different low emission zone

policy specifications, or public transport fare optimisation.

CRediT authorship contribution statement

Lawrence Christopher Duncan: Writing – review & editing, Writing – original draft, Visualization, Software, Methodology, Investigation, Funding acquisition, Formal analysis, Data curation, Conceptualization. **Thomas Kjær Rasmussen:** Writing – review & editing, Supervision, Software, Project administration, Methodology, Funding acquisition, Data curation, Conceptualization. **David Paul Watling:** Writing – review & editing, Methodology. **Ravi Seshadri:** Writing – review & editing, Methodology.

Declaration of competing interest

The authors declare that they have no known competing financial interests or personal relationships that could have appeared to influence the work reported in this paper.

Acknowledgements

We gratefully acknowledge the funding provided by the Independent Research Fund Denmark for the project “Optimal tolls for reaching emissions goals: A novel behaviourally realistic and national-scale applicable road transport modelling system” [Grant ID: 0217-00173B].

Appendix A. Nomenclature

Table 2 details the main nomenclature used in this paper. Note that the nomenclature for the model parameters are detailed in Appendix D.

Table 2
Nomenclature used in this paper.

Term	Description
Dynamic multi-region MFD SUE model	
R	Set of regions
n_r	Accumulation in region r
$W_r(n_r)$	Production-MFD function for region r given accumulation n_r
$v_r(n_r)$	Speed-MFD function for region r given accumulation n_r (space-mean speed)
M	Set of regional OD movements
P_m	Set of regional paths for OD movement m
N_m	Number of regional paths for OD movement m
N	Total number of regional paths
$R_{m,p}$	Set of regions in regional path p of OD movement m
Ψ	Set of indexed time-slices
ε	Time-slice duration
d_m^τ	Travel demand for OD movement m departing during time-slice τ
$f_{m,p}^\tau$	Vehicle flow departing during time-slice τ travelling regional path p of OD movement m
F	Set of all demand-feasible non-negative regional path flow vector solutions
$l_{m,p,r}$	Mean regional trip length of region r when travelling regional path p of OD movement m
$t_{m,p,r}^\tau$	Mean travel time to cross region r when entering the region during time-slice τ travelling regional path p of OD movement m
$\boldsymbol{t}^*(\boldsymbol{f})$	Region travel time vector solution to the traffic propagation fixed-point problem
$\overline{n}_{m,p,r}^{\tau' \to \tau}$	Average accumulation in region r during time-slice τ from the flow departing during time-slice τ' travelling regional path p of OD movement m
$\Psi_{m,p,r}^\tau$	Set of active time-slices that some time is spent in traversing region r by any vehicle departing during time-slice τ travelling regional path p of OD movement m
$\overline{t}_{m,p,r}^\tau$	Average travel time experienced to cross region r when departing during time-slice τ travelling regional path p of OD movement m
$\overline{T}_{m,p}^\tau$	Experienced travel time of regional path p of OD movement m when departing during time-slice τ under the NTS
$c_{m,p,r}^\tau$	Generalised travel cost to cross region r when departing during time-slice τ travelling regional path p of OD movement m
$C_{m,p,r}^\tau$	Generalised travel cost of regional path p of OD movement m when departing during time-slice τ
$Q_{m,p}^\tau$	Probability regional path p of OD movement m is chosen when departing during time-slice τ
Tolling	
$\kappa_{m,p,r}^\tau$	Toll paid in for travelling in region r when travelling regional path p of OD movement m and departing during time-slice τ
ω_r^τ	Time-based toll-price for travelling in region r during time-slice τ
$\mathrm{K}_{m,p}^\tau$	Total average time-based toll experienced when travelling regional path p of OD movement m and departing during time-slice τ
Elastic demand	
$Q_{m,p}^{\tau,NTS}$	Probability regional path p of OD movement m is chosen when departing during time-slice τ under the NTS
$C_{m,p}^{\tau,NTS}$	Generalised travel cost of regional path p of OD movement m when departing during time-slice τ under the NTS
$\widetilde{C}_m^\tau$	Level of service (expected travel cost) of OD movement m when departing during time-slice τ

(*continued on next page*)

Table 2 (*continued*)

Term	Description
$\widetilde{C}_m^{\tau,NTS}$	Level of service (expected travel cost) of OD movement m when departing during time-slice τ under the NTS
$\widetilde{d}_m^{\tau}$	Elastic demand for OD movement m departing during time-slice τ
Departure time choice	
$Y_m^{\tau' \to \tau}$	OD movement m utility of departing during time-slice τ in the TS given the traveller departed during time-slice τ' under the NTS
$PAT_m^{\tau,NTS}$	OD movement m aggregate preferred arrival time when departing during time-slice τ in the NTS
AT_m^{τ}	OD movement m aggregate arrival time when departing during time-slice τ in the TS
$\overline{T}_{m,p}^{\tau,NTS}$	Experienced travel time of regional path p of OD movement m when departing during time-slice τ under the NTS
$\overline{T}_m^{\tau}$	Average experienced travel of OD movement m when departing during time-slice τ
$\overline{T}_m^{\tau,NTS}$	Average experienced travel of OD movement m when departing during time-slice τ under the NTS
K_m^{τ}	Average toll experienced when departing during time-slice τ travelling OD movement m
$\pi_m^{\tau' \to \tau}$	Probability time-slice τ is chosen for travellers travelling OD movement m, given they depart during time-slice τ under the NTS
$\widetilde{d}_m^{\tau,DTC}$	Demand for OD movement m departing during time-slice τ, after elastic demand and departure time choice
Social welfare	
Z_{SW}	Social welfare objective function
Z_{ID}	Inverse demand component of the social welfare objective function
Z_{LoS}	Level of service component of the social welfare objective function
Z_{TR}	Toll revenue component of the social welfare objective function

Appendix B. Impact of scaling the producer component of the social welfare objective function

Here we shall explore the implications if we were to suppose that the toll revenues received by the governing authority are not fully reinvested or do not benefit society in an equivalent manner to the disbenefit from paying the tolls. We do this by scaling the producer component of the social welfare objective function in (20) by λ (i.e. $Z_{TR} = \lambda Z_{TR}$, $\lambda \in [0,1]$). Table 3 displays the optimal toll-price and gain in social welfare for different values of λ. As expected, the maximum gain in social welfare from tolling lessens as the value of the toll revenues to society is diminished. These maximum gains come from lower toll-prices, where after a certain point there is no benefit to society from tolling.

Such analysis could be useful to governing authorities, as if they have some perception of how beneficial the reinvested tolls might be back to society then they could correct their social welfare function accordingly, as we have done. An alternative analysis could be to assess, given our optimised toll price with $\lambda = 1$, how beneficial do our reinvested tolls need to be to society for the tolling to be beneficial. This is done by calculating the social welfare function with the outputs from the traffic model with the optimal toll-price when maximising with $\lambda = 1$, but scaling down the producer component by λ'. Table 4 displays the results from doing exactly such. As can be seen, the gains reduce quicker than when also optimising the toll-price accordingly (i.e. comparing with the results in Table 3). The conclusion is that as long as the toll revenues are reinvested to benefit society 90.1 % as much as the disbenefit from paying them, then tolling at a price 4.544 DKK/min will be worth it. This value can be calculated analytically by computing $(-Z_{ID} - Z_{LoS})/Z_{TR}$ (i.e. solving $Z_{SW} = 0 = Z_{ID} + Z_{LoS} + \lambda' Z_{TR}$).

Table 3
Toll-price optimisation results for different values of λ scaling the producer component of the social welfare objective function.

λ	0.8	0.85	0.9	0.95	1
Optimal Toll-Price [DKK/min]	0	0.523	1.650	3.094	4.544
Daily Gain in Social Welfare from NTS [DKK]	0	89,612	661,455	1,735,618	3,212,034
Net Benefit to Revenue Ratio	–	0.02	0.04	0.07	0.10

Table 4
Given the optimal toll-price from $\lambda = 1$, gain in social welfare for different values of λ' scaling the producer component of the social welfare objective function.

λ'	0.9	0.925	0.95	0.975	1
Daily Gain in Social Welfare from NTS [DKK]	−35,477	776,401	1,588,279	2,400,157	3,212,034

Appendix C. Demonstration of optimising multiple toll-prices

Fig. 25 displays a multi-region system that depicts a city centre and peripheral regions, inspired by similar multi-region systems in e.g. Zheng & Geroliminis (2020), Sirmatel & Yildirimoglu (2023). The idea is to model a morning commute where there are simplified demand movements. Demand travels within R1, from R2 to R1, and between each of the three outer periphery regions (R3-5). To travel between each pair of outer regions there are three regional paths as demonstrate in Fig. 25 between R5 and R4: one going through the city centre (RP1), one through middle region (RP2), and one remaining in the periphery regions (RP3). The city centre and middle regions (R1 & R2) will be toll to travel in between 7 and 9am, each with a different toll-price. We will not give all the details of the

specifications of the set-up and model, but essentially we have tried to create a set-up that is somewhat realistic. The demand profile is bell-shape-like representing the morning peak, and the city centre is heavily congested during the peak hours. The purpose of the tolls are to reduce congestion in the city centre, by encouraging travellers to diverting away from the city centre, depart earlier or later, or not travel by car at all.

Fig. 26A displays the toll-prices and social welfare objective function value at each iteration of the L-BFGS-B algorithm, solving with the D-MR-MFD-SUE with elastic demand and departure time choice model. As shown, the algorithm successfully identifies the toll-prices that maximise social welfare, which are 1.31 DKK/min and 2.51 DKK/min for R1 and R2, respectively. Fig. 26B displays the social welfare objective function surface. As can be seen the surface is smooth and has a unique maximum.

Regarding behaviour, Fig. 27A displays the change in demand departing at each 30-minute time-slice across the morning, which shows demand now departs earlier, or not at all by car. Fig. 27B displays the change in regional path choice probabilities for OD movement R5 → R4, where some diverting away from the city centre can be observed. These changes in behaviour lead to the congestion in R1 reducing dramatically during the peak hours, as displayed in Fig. 27C.

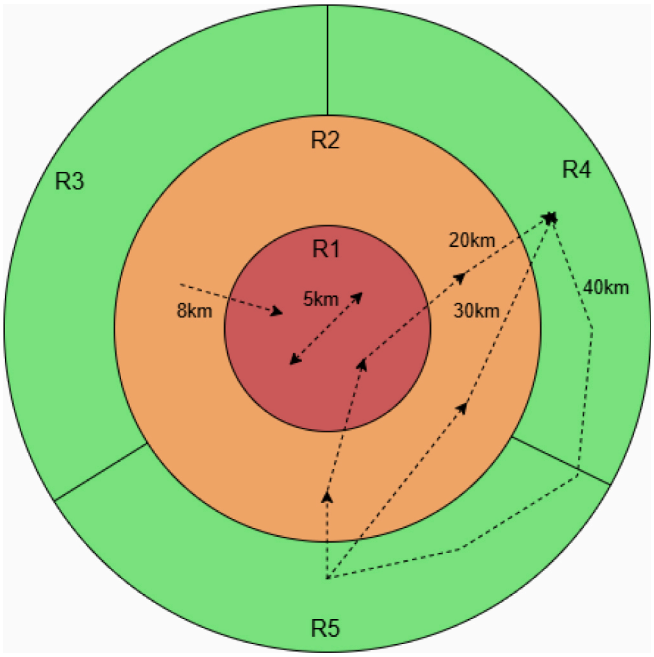

Fig. 25. City centre and periphery multi-region system.

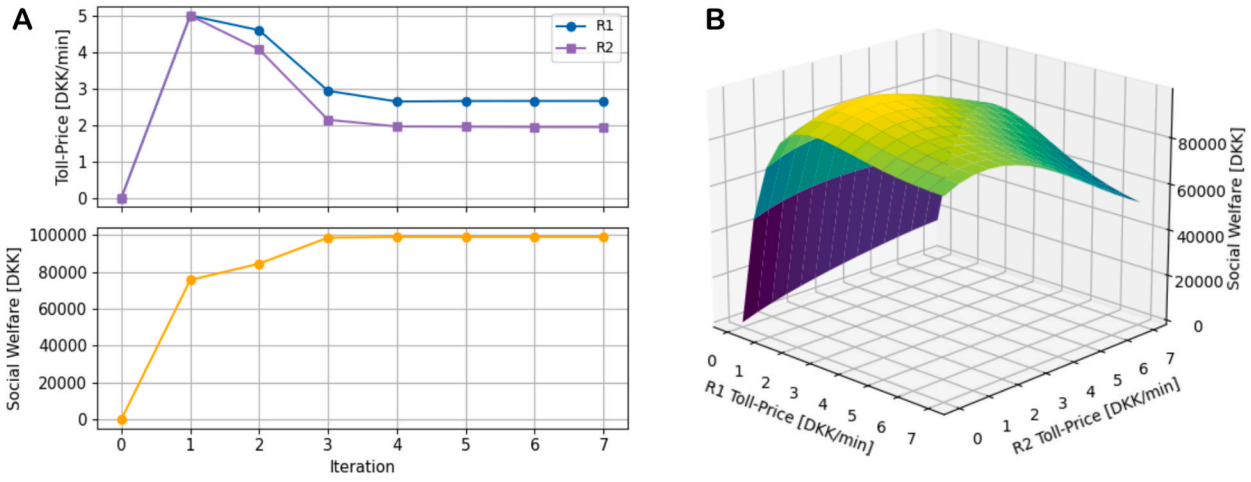

Fig. 26. A: Convergence of the toll-price optimisation algorithm to the optimal solution. B: Social welfare objective function surface.

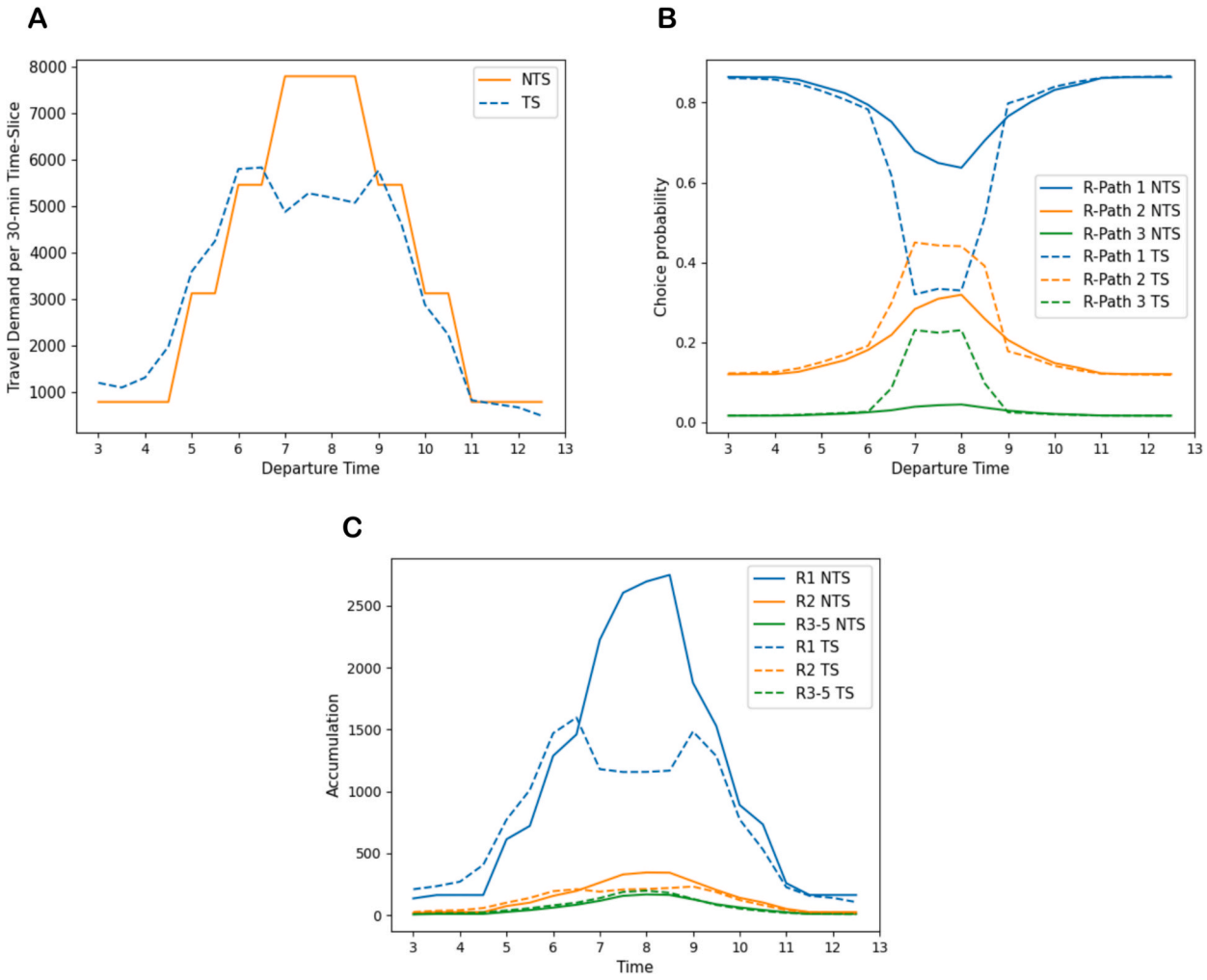

Fig. 27. Changes in behaviour between NTS and TS across the morning. A: Change in travel demand. B: Change in choice probability for the three regional paths travelling R4 R5. C: Change in accumulation in the regions.

Appendix D. Observed data and setting of model parameters

Table 5 gives an overview of all the model parameters we specified in the case study, including the data we observed and method we adopted to determine them.

Table 5
Overview of all model parameters.

Component of the model	Mathematical form	Parameter	Interpretation	Observed Data and Method of Determination
Underlying region speed-MFD functions	Exponential function	a	Free-flow speed	Calibrated by fitting the function to a set of speed-accumulation datapoints, obtained using a set of GPS traces of cars, and loop detector data to estimate the penetration rate (see Section 5.2 in Duncan et al. (2025))
		b	Curve	
		h	Minimum speed	
Motorway region speed-MFD functions	Piecewise-exponential form	a	Free-flow speed	
		n^{crit}	Critical accumulation	
		b	Curve pre-critical accumulation	
		c	Curve post-critical accumulation	
		h	Minimum speed	
Regional path choice model	C-Logit	θ	Logit scaling parameter measuring level of stochasticity in regional path choice / sensitivity to differences in regional path utility	Calibrated through maximum likelihood estimation using a set of GPS traces of cars (see Section 6 in Duncan et al. (2025))
		$\alpha_{l/tt}$	Relative value of distance to time, measuring how much further a driver is willing to travel to save 1 min of travel time	
		ν	C-Logit commonality scaling parameter, measuring sensitivity to regional path similarity	
Elastic demand	Power law function	γ	Demand elasticity parameter for car, measuring demand sensitivity to changes in the LoS for car	Parameter value has been taken from the Danish national transport model, which has been estimated based on a Danish national travel survey. The model framework is described in Rich & Hansen (2016).
Departure time choice model	Multinomial Logit	μ	Logit scaling parameter measuring level of stochasticity in departure time choice / sensitivity to differences in departure time utility	Determined through manual experimentation, balancing sensitivity to changes in departure time-slice utilities (e.g. with tolls) against reproducing the original demand profile before in Rasmussen et al. (2021) (demand from an operational Danish national transport model calibrated against the national travel survey)
		α_{tt}	Value of time, measuring monetary worth of 1 min of travel time	Determined by taking the value of distance from the official Danish transport economic unit price catalogue (Transportministeriet, 2024) and combining with our estimated relative value of distance to time (see for $\alpha_{l/tt}$ above)
		$\frac{\alpha^{\tau}_{early}}{\alpha_{tt}}$	Relative value of arriving early compared to value of time, measuring how much more travel time a driver is willing to accept to avoid arriving 1 min early	Values taken from Small (1982), a study that estimates how commuters trade off schedule delays (arriving early/late) against travel time and cost, based on a travel survey
		$\frac{\alpha^{\tau}_{late}}{\alpha_{tt}}$	Relative value of arriving late compared to value of time, measuring how much more travel time a driver is willing to accept to avoid arriving 1 min late	

Data availability

We do not have permission to share the data, but the code can be shared upon request.

References

Abkowitz M, (1980). The impact of service reliability on work travel behavior. Doctoral dissertation, Massachusetts Institute of Technology.

Aboudina, A., Abdelgawad, H., Abdulhai, B., Habib, K., 2016. Time-dependent congestion pricing system for large networks: Integrating departure time choice, dynamic traffic assignment and regional travel surveys in the Greater Toronto Area. Transp. Res. A Policy Pract. 94, 411–430.

Alisoltani, N., Leclercq, L., Zargayouna, M., 2021. Can dynamic ride-sharing reduce traffic congestion? Transp. Res. B Methodol. 145, 212–246.

Alisoltani, N., Zargayouna, M., Leclercq, L., 2020. A sequential clustering method for the taxi-dispatching problem considering traffic dynamics. IEEE Intell. Transp. Syst. Mag. 12 (4), 169–181.

Amirgholy, M., Gao, H., 2017. Modeling the dynamics of congestion in large urban networks using the macroscopic fundamental diagram: User equilibrium, system optimum, and pricing strategies. Transp. Res. B Methodol. 104, 215–237.

Arnott, R., 2013. A bathtub model of downtown traffic congestion. J. Urban Econ. 76, 110–121.

Arnott, R., de Palma, A., Lindsey, R., 1990. Departure time and route choice for the morning commute. Transp. Res. B Methodol. 24 (3), 209–228.

Balzer, L., Leclercq, L., 2022. Modal equilibrium of a tradable credit scheme with a trip-based MFD and logit-based decision-making. Transp. Res. Part C Emerging Technol. 139, 103642.

Balzer, L., Ameli, M., Leclercq, L., Lebacque, J., 2023. Dynamic tradable credit scheme for multimodal urban networks. Transp. Res. Part C Emerging Technol. 149, 104061.

Barmpounakis, E., Montesinos-Ferrer, M., Gonzales, E., Geroliminis, N., 2021. Empirical investigation of the emission-macroscopic fundamental diagram. Transp. Res. Part D: Transp. Environ. 101, 103090.

Batista, S., Leclercq, L., 2020. Regional dynamic traffic assignment with bounded rational drivers as a tool for assessing the emissions in large metropolitan areas. Transp. Res. Interdiscip. Perspect. 8, 100248.

Batista, S., Ingole, D., Leclercq, L., Menéndez, M., 2021. The role of trip lengths calibration in model-based perimeter control strategies. IEEE Trans. Intell. Transp. Syst. 23 (6), 5176–5186.

Batista, S., Tilg, G., Menéndez, M., 2022. Exploring the potential of aggregated traffic models for estimating network-wide emissions. Transp. Res. Part D: Transp. Environ. 109, 103354.

Beojone, C., Geroliminis, N., 2021. On the inefficiency of ride-sourcing services towards urban congestion. Transp. Res. Part C Emerging Technol. 124, 102890.

Byrd, R., Lu, P., Nocedal, J., Zhu, C., 1995. A limited memory algorithm for bound constrained optimization. SIAM J. Sci. Comput. 16 (5), 1190–1208.

Cantelmo, G., Viti, F., 2019. Incorporating activity duration and scheduling utility into equilibrium-based Dynamic Traffic Assignment. Transp. Res. B Methodol. 126, 365–390.

Cascetta, E., Nuzzolo, A., Russo, F., Vitetta, A., 1996. A modified logit route choice model overcoming path overlapping problems: specification and some calibration results for inter-urban networks. In: In: Proceedings of the 13th International Symposium on Transportation and Traffic Theory, pp. 697–711.

Chen, X., Xiong, C., He, X., Zhu, Z., Zhang, L., 2016. Time-of-day vehicle mileage fees for congestion mitigation and revenue generation: a simulation-based optimization method and its real-world application. Transp. Res. Part C Emerging Technol. 63, 71–95.

Chen, Y., Zheng, N., Vu, H., 2021. A novel urban congestion pricing scheme considering travel cost perception and level of service. Transp. Res. Part C Emerging Technol. 125, 103042.

Chen, C., Huang, Y., Lam, W., Pan, T., Hsu, S., Sumalee, A., Zhong, R., 2022. Data efficient reinforcement learning and adaptive optimal perimeter control of network traffic dynamics. Transp. Res. Part C Emerging Technol. 142, 103759.

Chen, C., Geroliminis, N., Zhong, R., 2024. An iterative adaptive dynamic programming approach for macroscopic fundamental diagram-based perimeter control and route guidance. Transp. Sci. 58 (4), 896–918.

Chen, Y., Gu, Z., Zheng, N., Vu, H.L., 2024. Optimal coordinated congestion pricing for multiple regions: a surrogate-based approach. Transportation 51 (6), 2139–2171.

Cheng, Q., Liu, Z., Liu, F., Jia, R., 2017. Urban dynamic congestion pricing: an overview and emerging research needs. Int. J. Urban Sci. 21 (sup1), 3–18.

Daganzo, C., 2007. Urban gridlock: macroscopic modeling and mitigation approaches. Transp. Res. B Methodol. 41 (1), 49–62.

Daganzo, C., Lehe, L., 2015. Distance-dependent congestion pricing for downtown zones. Transp. Res. B Methodol. 75, 89–99.

Dantsuji, T., Fukuda, D., Zheng, N., 2021. Simulation-based joint optimization framework for congestion mitigation in multimodal urban network: a macroscopic approach. Transportation 48, 673–697.

Ding, H., Wang, L., Zheng, N., Cheng, Z., Zheng, X., Li, J., 2025. A novel hierarchical perimeter control method for road networks considering boundary congestion in a mixed CAV and HV traffic environment. Transp. Res. B Methodol. 195, 103219.

Duncan, L., Rasmussen, T., Watling, D., Nielsen, O., 2025. Dynamic multi-region MFD stochastic user equilibrium: formulation and parameter estimation in a large-scale case study. Transp. Res. Part C Emerging Technol. 173, 105008. https://doi.org/10.1016/j.trc.2025.105008.

Eliasson, J., 2009. A cost–benefit analysis of the Stockholm congestion charging system. Transp. Res. A Policy Pract. 43 (4), p,468–480.

Eliasson, J., Mattsson, L., 2006. Equity effects of congestion pricing: quantitative methodology and a case study for Stockholm. Transp. Res. A Policy Pract. 40 (7), 602–620.

Fosgerau, M., 2015. Congestion in the bathtub. Econ. Transp. 4 (4), 241–255.

Fu, H., Chen, S., Chen, K., Kouvelas, A., Geroliminis, N., 2021. Perimeter control and route guidance of multi-region mfd systems with boundary queues using colored petri nets. IEEE Trans. Intell. Transp. Syst. 23 (8), 12977–12999.

Genser, A., Kouvelas, A., 2022. Dynamic optimal congestion pricing in multi-region urban networks by application of a Multi-Layer-Neural network. Transp. Res. Part C Emerging Technol. 134, 103485.

Geroliminis, N., Daganzo, C., 2008. Existence of urban-scale macroscopic fundamental diagrams: some experimental findings. Transp. Res. B 42 (9), 759–770.

Geroliminis, N., Haddad, J., Ramezani, M., 2012. Optimal perimeter control for two urban regions with macroscopic fundamental diagrams: a model predictive approach. IEEE Trans. Intell. Transp. Syst. 14 (1), 348–359.

Geroliminis, N., Levinson, D., 2009. Cordon pricing consistent with the physics of overcrowding. In: Transportation and Traffic Theory 2009: Golden Jubilee: Papers Selected for Presentation at ISTTT18, a Peer Reviewed Series since 1959. Springer, US, Boston, MA, pp. 219–240.

Gu, Z., Liu, Z., Cheng, Q., Saberi, M., 2018. Congestion pricing practices and public acceptance: a review of evidence. Case Studies on Transport Policy 6 (1), 94–101.

Gu, Z., Shafiei, S., Liu, Z., Saberi, M., 2018. Optimal distance-and time-dependent area-based pricing with the Network Fundamental Diagram. Transp. Res. Part C Emerging Technol. 95, 1–28.

Gu, Z., Waller, S., Saberi, M., 2019. Surrogate-based toll optimization in a large-scale heterogeneously congested network. Comput. Aided Civ. Inf. Eng. 34 (8), 638–653.

Guo, Q., Ban, X., 2020. Macroscopic fundamental diagram based perimeter control considering dynamic user equilibrium. Transp. Res. B Methodol. 136, 87–109.

Gu, Z., Saberi, M., 2021. Simulation-based optimization of toll pricing in large-scale urban networks using the network fundamental diagram: a cross-comparison of methods. Transp. Res. Part C Emerging Technol. 122, 102894.

Haddad, J., Ramezani, M., Geroliminis, N., 2013. Cooperative traffic control of a mixed network with two urban regions and a freeway. Transp. Res. B Methodol. 54, 17–36.

Haddad, J., 2017a. Optimal coupled and decoupled perimeter control in one-region cities. Control Eng. Pract. 61, 134–148.

Haddad, J., 2017b. Optimal perimeter control synthesis for two urban regions with aggregate boundary queue dynamics. Transp. Res. B Methodol. 96, 1–25.

Hamedmoghadam, H., Zheng, N., Li, D., Vu, H., 2022. Percolation-based dynamic perimeter control for mitigating congestion propagation in urban road networks. Transp. Res. Part C Emerging Technol. 145, 103922.
Hansson I, (1985). Marginal cost of public funds for different tax instruments and government expenditures. In: Limits and Problems of Taxation, p.17-32.
He, Z., Han, Y., Ji, X., Yu, H., Liu, P., Kouvelas, A., 2024. Hierarchical perimeter control with network heterogeneity reduction and queue management. IEEE Intell. Transp. Syst. Mag.
Hosseinzadeh, F., Moshahedi, N., Kattan, L., 2023. An MFD approach to route guidance with consideration of fairness. Transp. Res. Part C Emerging Technol. 157, 104359.
Huang, H., Yang, H., Bell, M., 2000. The models and economics of carpools. Ann. Reg. Sci. 34, 55–68.
Huang, Y., Xiong, J., Sumalee, A., Zheng, N., Lam, W., He, Z., Zhong, R., 2020. A dynamic user equilibrium model for multi-region macroscopic fundamental diagram systems with time-varying delays. Transp. Res. B Methodol. 131, 1–25.
Isaacson, E., Keller, H., 1966. Analysis of Numerical Methods. John Wiley & Sons Inc, New York, USA.
Jiang, S., Keyvan-Ekbatani, M., 2023. Hybrid perimeter control with real-time partitions in heterogeneous urban networks: an integration of deep learning and MPC. Transp. Res. Part C Emerging Technol. 154, 104240.
Jiang, S., Tran, C., Keyvan-Ekbatani, M., 2024. Regional route guidance with realistic compliance patterns: Application of deep reinforcement learning and MPC. Transp. Res. Part C Emerging Technol. 158, 104440.
Jing, P., Seshadri, R., Sakai, T., Shamshiripour, A., Alho, A., Lentzakis, A., Ben-Akiva, M., 2024. Evaluating congestion pricing schemes using agent-based passenger and freight microsimulation. Transp. Res. A Policy Pract. 186, 104118.
Joksimovic, D., Bliemer, M., Bovy, P., 2005. Optimal toll design problem in dynamic traffic networks with joint route and departure time choice. Transp. Res. Rec. 1923 (1), 61–72.
Keyvan-Ekbatani, M., Kouvelas, A., Papamichail, I., Papageorgiou, M., 2012. Exploiting the fundamental diagram of urban networks for feedback-based gating. Transp. Res. B Methodol. 46 (10), 1393–1403.
Keyvan-Ekbatani, M., Papageorgiou, M., Knoop, V., 2015a. Controller design for gating traffic control in presence of time-delay in urban road networks. Transp. Res. Part C Emerging Technol. 59, 308–322.
Keyvan-Ekbatani, M., Yildirimoglu, M., Geroliminis, N., Papageorgiou, M., 2015b. Multiple concentric gating traffic control in large-scale urban networks. IEEE Trans. Intell. Transp. Syst. 16 (4), 2141–2154.
Keyvan-Ekbatani, M., Carlson, R., Knoop, Papageorgiou, M., 2021. Optimizing distribution of metered traffic flow in perimeter control: Queue and delay balancing approaches. Control Eng. Pract. 110, 104762.
Knoop, V., Hoogendoorn, S., Van Lint, J., 2012. Routing strategies based on macroscopic fundamental diagram. Transp. Res. Rec. 2315 (1), 1–10.
Koh, A., Shepherd, S., Watling, D., 2013. Competition between two cities using cordon tolls: an exploration of response surfaces and possibilities for collusion. Transportmetrica a: Transp. Sci. 9 (10), 896–924.
Kouvelas, A., Saeedmanesh, M., Geroliminis, N., 2023. A linear-parameter-varying formulation for model predictive perimeter control in multi-region MFD urban networks. Transp. Sci. 57 (6), 1496–1515.
Lamotte R & Geroliminis N, (2016). The morning commute in urban areas: insights from theory and simulation (No. 16-2003).
Leclercq, L., Sénécat, A., Mariotte, G., 2017. Dynamic macroscopic simulation of on-street parking search: a trip-based approach. Transp. Res. B Methodol. 101, 268–282.
Lehe, L., 2017. Downtown tolls and the distribution of trip lengths. Econ. Transp. 11, 23–32.
Lentzakis, A., Seshadri, R., Akkinepally, A., Vu, V., Ben-Akiva, M., 2020. Hierarchical density-based clustering methods for tolling zone definition and their impact on distance-based toll optimization. Transp. Res. Part C Emerging Technol. 118, 102685.
Liu, Z., Wang, S., Zhou, B., Cheng, Q., 2017. Robust optimization of distance-based tolls in a network considering stochastic day to day dynamics. Transp. Res. Part C Emerging Technol. 79, 58–72.
Lombardi, C., Picado-Santos, L., Annaswamy, A., 2021. Model-based dynamic toll pricing: an overview. Appl. Sci. 11 (11), 4778.
Lu, C., Mahmassani, H., Zhou, X., 2008. A bi-criterion dynamic user equilibrium traffic assignment model and solution algorithm for evaluating dynamic road pricing strategies. Transp. Res. Part C Emerging Technol. 16 (4), 371–389.
Mahmassani, H., Herman, R., 1984. Dynamic user equilibrium departure time and route choice on idealized traffic arterials. Transp. Sci. 18 (4), 362–384.
Mansourianfar, M., Gu, Z., Waller, S., Saberi, M., 2021. Joint routing and pricing control in congested mixed autonomy networks. Transp. Res. Part C Emerging Technol. 131, 103338.
Mansourianfar, M., Gu, Z., Saberi, M., 2024. Joint routing and pricing control in bimodal mixed autonomy networks with elastic demand and three-dimensional passenger macroscopic fundamental diagram. Transp. Res. Rec., 03611981241243080
Mariotte, G., Leclercq, L., Laval, J., 2017. Macroscopic urban dynamics: analytical and numerical comparisons of existing models. Transp. Res. B Methodol. 101, 245–267.
Menelaou, C., Timotheou, S., Kolios, P., Panayiotou, C., 2023. Convexification approaches for regional route guidance and demand management with generalized MFDs. Transp. Res. Part C Emerging Technol. 154, 104245.
Meng, Q., Liu, Z., Wang, S., 2012. Optimal distance tolls under congestion pricing and continuously distributed value of time. Transp. Res. Part E: Logistics and Transp. Rev. 48 (5), 937–957.
Qian, Y., Ding, H., Meng, Y., Zheng, N., Di, Y., Zheng, X., 2024. Combination of H∞ perimeter control and route guidance for heterogeneous urban road networks. TransportmetricaB: Transport Dynamics 12 (1), 2359025.
de Palma, A., Ben-Akiva, M., Lefevre, C., Litinas, N., 1983. Stochastic equilibrium model of peak period traffic congestion. Transp. Sci. 17 (4), 430–453.
de Palma, A., Kilani, M., Lindsey, R., 2005. Congestion pricing on a road network: a study using the dynamic equilibrium simulator METROPOLIS. Transp. Res. A Policy Pract. 39 (7–9), 588–611.
de Palma, A., Lindsey, R., 2011. Traffic congestion pricing methodologies and technologies. Transp. Res. Part C Emerging Technol. 19 (6), 1377–1399.
Parishad, N., Yildirimoglu, M., Hickman, M., 2025. Congestion pricing in multi-modal networks: an application of deep reinforcement learning. Transp. Res. Part C Emerging Technol. 177, 105166.
Rambha, T., Boyles, S., 2016. Dynamic pricing in discrete time stochastic day-to-day route choice models. Transp. Res. B Methodol. 92, 104–118.
Ramezani, M., Haddad, J., Geroliminis, N., 2015. Dynamics of heterogeneity in urban networks: aggregated traffic modeling and hierarchical control. Transp. Res. B Methodol. 74, 1–19.
Ramezani, M., Nourinejad, M., 2018. Dynamic modeling and control of taxi services in large-scale urban networks: a macroscopic approach. Transp. Res. Part C Emerging Technol. 94, 203–219.
Ramezani, M., Valadkhani, A., 2023. Dynamic ride-sourcing systems for city-scale networks-Part I: matching design and model formulation and validation. Transp. Res. Part C Emerging Technol. 152, 104158.
Rasmussen T, Brun B, & Hansen C, (2021). Dynamic Traffic Assignment in a large-scale transport model (COMPASS). Proceedings of Trafikdage, August 23-24, Aalborg Denmark.
Ren, Y., Hou, Z., Sirmatel, I., Geroliminis, N., 2020. Data driven model free adaptive iterative learning perimeter control for large-scale urban road networks. Transp. Res. Part C Emerging Technol. 115, 102618.
Rich, J., Hansen, C., 2016. The danish national passenger model – model specification and results. Eur. J. Transp. Infrastruct. Res. 16 (4), p,573–599.
Rich, J., Nielsen, O., 2007. A socio-economic assessment of proposed road user charging schemes in Copenhagen. Transp. Policy 14 (4), 330–345.
Simoni M, Pel A, Waraich R, & Hoogendoorn S, (2014). Congestion pricing based on dynamic features of the Macroscopic Fundamental Diagram. Arbeitsberichte Verkehrs-und Raumplanung, 1000.
Sirmatel, I., Geroliminis, N., 2021. Stabilization of city-scale road traffic networks via macroscopic fundamental diagram-based model predictive perimeter control. Control Eng. Pract. 109, 104750.

Sirmatel, I., Tsitsokas, D., Kouvelas, A., Geroliminis, N., 2021. Modeling, estimation, and control in large-scale urban road networks with remaining travel distance dynamics. Transp. Res. Part C Emerging Technol. 128, 103157.
Sirmatel, I., Yildirimoglu, M., 2023. Nonlinear model predictive control of large-scale urban road networks via average speed control. Transp. Res. Part C Emerging Technol. 156, 104338.
Small, K., 1982. The scheduling of consumer activities: work trips. Am. Econ. Rev. 72 (3), 467–479.
de Souza, F., Saucedo, R., Mousavizadeh, O., Carlson, R., Keyvan-Ekbatani, M., 2024. On the evaluation and selection of network-level traffic control policies: perimeter control, TUC, and their combination. Transp. Res. A Policy Pract. 186, 104161.
Steed J & Bhat C, (2000). Modeling departure time choice for home-based non-work trips (No. SWUTC/00/167500-1). Southwest Region University Transportation Center, Center for Transportation Research, University of Texas.
Szeto, W., Lo, H., 2004. A cell-based simultaneous route and departure time choice model with elastic demand. Transp. Res. B Methodol. 38 (7), 593–612.
Transportministeriet, (2024). Transportøkonomiske Enhedspriser til brug for samfundsøkonomiske analyser – version 2.1. Unit price catalogue, downloaded from https://www.man.dtu.dk/myndighedsbetjening/teresa-og-transportoekonomiske-enhedspriser, accessed 04/12/2024.
Tsitsokas, D., Kouvelas, A., Geroliminis, N., 2023. Two-layer adaptive signal control framework for large-scale dynamically-congested networks: combining efficient max pressure with perimeter control. Transp. Res. Part C Emerging Technol. 152, 104128.
Valadkhani, A., Ramezani, M., 2023. Dynamic ride-sourcing systems for city-scale networks, part II: proactive vehicle repositioning. Transp. Res. Part C Emerging Technol. 152, 104159.
Verhoef, E., Nijkamp, P., Rietveld, P., 1996. Second-best congestion pricing: the case of an untolled alternative. J. Urban Econ. 40 (3), 279–302.
Wang, X., Gayah, V., 2021. Cordon-based pricing schemes for mixed urban-freeway networks using macroscopic fundamental diagrams. Transp. Res. Rec. 2675 (10), 1339–1351.
Watling, D., Shepherd, S., Koh, A., 2015. Cordon toll competition in a network of two cities: formulation and sensitivity to traveller route and demand responses. Transp. Res. B Methodol. 76, 93–116.
Wei, B., Sun, D., 2018. A two-layer network dynamic congestion pricing based on macroscopic fundamental diagram. J. Adv. Transp. 2018 (1), 8616120.
Yang, H., 1999. System optimum, stochastic user equilibrium, and optimal link tolls. Transp. Sci. 33 (4), 354–360.
Yang, H., Bell, M., 1997. Traffic restraint, road pricing and network equilibrium. Transp. Res. B Methodol. 31 (4), 303–314.
Yang, H., Meng, Q., 1998. Departure time, route choice and congestion toll in a queuing network with elastic demand. Transp. Res. B Methodol. 32 (4), 247–260.
Yang, H., Meng, Q., 2000. Highway pricing and capacity choice in a road network under a build–operate–transfer scheme. Transp. Res. A Policy Pract. 34 (3), 207–222.
Yildirimoglu, M., Ramezani, M., Geroliminis, N., 2015. Equilibrium analysis and route guidance in large-scale networks with MFD dynamics. Transp. Res. Procedia 9, 185–204.
Ying, J., Yang, H., 2005. Sensitivity analysis of stochastic user equilibrium flows in a bi-modal network with application to optimal pricing. Transp. Res. B Methodol. 39 (9), 769–795.
Yu, J., Laharotte, P., Han, Y., Ma, W., Leclercq, L., 2025. Perimeter control with heterogeneous metering rates for cordon signals: a physics-regularized multi-agent reinforcement learning approach. Transp. Res. Part C Emerging Technol. 171, 104944.
Zheng, N., Waraich, R., Axhausen, K., Geroliminis, N., 2012. A dynamic cordon pricing scheme combining the macroscopic fundamental diagram and an agent-based traffic model. Transp. Res. A Policy Pract. 46 (8), 1291–1303.
Zheng, N., Geroliminis, N., 2013. On the distribution of urban road space for multimodal congested networks. Procedia Soc. Behav. Sci. 80, 119–138.
Zheng, N., Geroliminis, N., 2016. Modeling and optimization of multimodal urban networks with limited parking and dynamic pricing. Transp. Res. B Methodol. 83, 36–58.
Zheng, N., Geroliminis, N., 2020. Area-based equitable pricing strategies for multimodal urban networks with heterogeneous users. Transp. Res. A Policy Pract. 136, 357–374.
Zheng, N., Rérat, G., Geroliminis, N., 2016. Time-dependent area-based pricing for multimodal systems with heterogeneous users in an agent-based environment. Transp. Res. Part C Emerging Technol. 62, 133–148.
Zhong, R., Chen, C., Huang, Y., Sumalee, A., Lam, W., Xu, D., 2018a. Robust perimeter control for two urban regions with macroscopic fundamental diagrams: a control-Lyapunov function approach. Transp. Res. B Methodol. 117, 687–707.
Zhong, R., Huang, Y., Chen, C., Lam, W., Xu, D., Sumalee, A., 2018b. Boundary conditions and behavior of the macroscopic fundamental diagram based network traffic dynamics: a control systems perspective. Transp. Res. B Methodol. 111, 327–355.
Zhong, R., Xiong, J., Huang, Y., Sumalee, A., Chow, A., Pan, T., 2020. Dynamic system optimum analysis of multi-region macroscopic fundamental diagram systems with state-dependent time-varying delays. IEEE Trans. Intell. Transp. Syst. 21 (9), 4000–4016.
Zhong, R., Xiong, J., Huang, Y., Zheng, N., Lam, W., Pan, T., He, B., 2021. Dynamic user equilibrium for departure time choice in the basic trip-based model. Transp. Res. Part C Emerging Technol. 128, 103190.
Zhu, C., Wen, G., Li, N., Bian, L., Wu, J., Kouvelas, A., 2023. Resilience enhancement of urban roadway network during disruption via perimeter control. IEEE Trans. Network Sci. Eng. 11 (1), 1227–1237.